Open access • Journal Article • DOI:10.1063/1.452099

Purely rotational coherence effect and time-resolved sub-Doppler spectroscopy of large molecules. II. Experimental

J. Spencer Baskin, Peter M. Felker, Ahmed H. Zewail

Published on: 01 Mar 1987 - Journal of Chemical Physics (American Institute of Physics)

Topics: Rotational temperature, Rotational–vibrational spectroscopy, Rotational transition, Rotational partition function and Rotational spectroscopy

Purely rotational coherence effect and time-resolved sub-Doppler spectroscopy of large molecules. I. Theoretical

Peter M. Felker[a] and Ahmed H. Zewail
Arthur Amos Noyes Laboratory of Chemical Physics,[b] *California Institute of Technology, Pasadena, California 91125*

(Received 3 November 1986; accepted 24 November 1986)

In this and the accompanying paper we present a theoretical treatment and experimental study, respectively, of the phenomenon termed *purely rotational coherence*. This phenomenon has been demonstrated to be useful as a time domain means by which to obtain high resolution spectroscopic information on excited state rotational levels of large molecules [Felker *et al.*, J. Phys. Chem. **90**, 724 (1986); Baskin *et al.*, J. Chem. Phys. **84**, 4708 (1986)]. Here, the manifestations in temporally resolved, *polarization-analyzed* fluorescence of coherently prepared rotational levels in samples of isolated symmetric and asymmetric top molecules are considered. These manifestations, for reasonably large molecules at rotational temperatures characteristic of jet-cooled samples, take the form of polarization-dependent transients and *recurrences* with temporal widths of the order of tens of picoseconds or less. The transients, which arise from the thermal averaging of many single molecule coherences, are examined with respect to their dependences on molecular parameters (rotational constants, transition dipole directions) and experimental parameters (polarization directions and temperature). A physical picture of rotational coherence as a reflection of the time-dependent orientation of molecules in the sample is developed. And. the influence of rotational coherence in experiments designed to probe intramolecular energy flow is discussed. In the accompanying paper, we present experimental results for jet-cooled *t*-stilbene and anthracene. For *t*-stilbene we determine rotational constants for vibrational levels in the S_1 electronic state (from the recurrences) and we monitor the trends in rotational coherence vs vibrational coherence as the total energy in the molecule increases.

I. INTRODUCTION

In two previous letters[1,2] we have reported on the theoretical prediction and experimental observation of effects associated with what we have termed *purely rotational coherence* in jet-cooled samples of large molecules. The situation of a purely rotational coherence arises when a molecule is subjected to a pulse of light of suitable frequency and bandwidth to excite a coherent superposition of rotational levels within a given vibronic manifold of the molecule. Such a coherent superposition state (like other types of superposition states), can give rise to quantum interference effects,[3] in particular quantum beat-modulated fluorescence decays. In Ref. 1 it was demonstrated for the first time that these interference effects associated with purely rotational coherence can be observable, even when subjected to the thermal averaging characteristic of experimentally realizable, gaseous samples of large molecules. In picosecond time-resolved fluorescence polarization experiments it is possible to observe recurrences in the fluorescence intensity vs time, which occur with temporal spacings related to the rotational level structure of the molecule.[1,2] The recurrences represent the thermal (incoherent) averaging of many single molecule rotational coherences. They reflect *rephasings in the alignment* of transition dipole moments of molecules in the sample, an effect reminiscent of the rephasing of oscillating dipoles that occurs in photon echo experiments.

The fact that rotational coherence effects can be observed in samples of molecules at finite temperature is important for several reasons. First, high resolution, sub-Doppler optical spectroscopy pertaining to the rotational level structure of large molecules is now possible through time domain measurements of rotational coherence effects. This point has already been demonstrated in Ref. 2, wherein measurements of the rotational constants of *t*-stilbene, *t*-stilbene-d_{12}, and *t*-stilbene–argon complexes were reported. A second reason is that the transients associated with rotational coherence are sensitive to the direction of the transition dipoles involved in excitation and detection. As such, the transients serve as a probe of these directions and, thus as a probe of the symmetries of the vibronic states involved. Third, rotational coherence effects, being ultimately a manifestation of the temporally changing orientation (in the nontechnical sense of the word) of vibronically excited molecules in the sample, may be expected to be quite sensitive to those *inter*molecular interactions that tend to perturb that alignment. Hence, the effects represent a means by which to probe the collisions that lead to the rotational relaxation of molecules. Finally, the existence of observable rotational coherence effects has implications with regard to time-resolved polarization studies of intramolecular energy flow.[1] Such studies[4–6] (as well as spectral domain measurements[7]) typically pertain to the assessment of the influence of molecular

[a] Present address: Department of Chemistry, University of California, Los Angeles, CA 91125.
[b] This work is supported by a grant from the National Science Foundation (DMR 85-21191). Contribution No. 7449.

 0021-9606/87/052460-23$02.10

rotation on the intramolecular dynamics arising from singlet–triplet interactions,[4] and on intramolecular vibrational energy redistribution (IVR).[5,6] However, the polarization-dependent transients associated with such intramolecular dynamics may be very similar in form to transients associated with purely rotational coherence.[1] One must therefore be cautious in interpreting the result of a time-resolved polarization experiment as the manifestation of some intramolecular dynamical process.

The consideration of purely rotational coherence in time-resolved experiments on isolated molecules is the purpose of this paper. (In a companion paper[8] we present experimental results that are pertinent to the theoretical results here.) Our concern is with characterizing the transients—time scale, magnitude, and dependences on molecular and experimental parameters—that can occur in the fluorescence decays of isolated molecule samples subsequent to pulsed laser preparation of coherent superpositions of rotational states. The intent is to generalize the theoretical results of Ref. 1 to account for (1) asymmetric as well as symmetric top molecules; (2) arbitrary absorption and emission dipole directions; (3) arbitrary excitation and detection polarizations, and (4) cases where rotational coherence effects *and* intramolecular energy flow processes contribute to observed transients. In addition, we shall examine the physical meaning of rotational coherence and how the phenomenon and its manifestations relate to classically rotating molecules.

The organization of the paper is as follows. We present first a brief description of purely rotational coherence and the effect which averaging over a thermal ensemble has on its observable manifestations. This section is meant as an introduction to the considerably more general results to be derived thereafter. The next section presents a theoretical framework with which general results pertaining to quantum interference effects in molecules can be derived. This framework is based on a density matrix/spherical tensor approach and is an adaptation to molecules of the methodology used by Silverman, Haroche, and Gross[9] to treat quantum interference effects in atoms. The two following sections pertain to purely rotational coherence effects in symmetric and asymmetric top molecules, respectively. For each case we present general results and the results of fluorescence decay calculations for specific, representative molecules. The topic of Sec. VI is the examination of a physical picture of rotational coherence effects as reflecting the time-dependent orientation of excited molecules in a gaseous sample. Section VII pertains to the temporally resolved fluorescence to be expected from classically rotating molecules. In this section it is shown that significant correspondences exist between classical and quantum mechanical results associated with rotational coherence. Finally, in the last section we examine the influence that rotational coherence has in decays that contain contributions from intramolecular dynamical processes. Of particular concern here is the situation wherein both rotational coherence, and the intramolecular vibrational energy redistribution (IVR) processes that arise from the anharmonic coupling of vibrational levels, contribute to the temporal evolution of fluorescence.

II. ELEMENTARY PICTURE OF ROTATIONAL COHERENCE EFFECTS

Before delving into a formal, density matrix treatment of rotational coherence, it is useful to develop a somewhat qualitative picture of the phenomenon,[1] so as to render subsequent mathematics more intelligible. Two essential aspects characterize rotational coherence effects in gaseous samples of molecules: (1) quantum interference between rotational levels of individual molecules, giving rise to quantum beat-modulated decays, and (2) the thermal averaging of these beat-modulated decays over the ensemble of molecules in the sample.

A. Rotational quantum beats

The general conditions under which generic, single species quantum beats arise are well known.[3] One must excite two or more eigenstates of a species via coherent, pulsed excitation from a single eigenstate. Such an excitation process creates a coherent superposition state composed of excited eigenstates having a well defined phase relationship with respect to one another. In probing this superposition state in time via a transition to some final state, quantum beat modulations in the probe signal arise *only* when two or more of the eigenstates comprising the superposition state can undergo transitions to the same final state *and* when these two or more "probe" transitions are actually monitored in the experiment. When the necessary excitation and detection conditions are met, sinusoidal temporal modulations (quantum beats) in the probe signal obtain. The beats, which reflect interferences between pairs of the eigenstates comprising the superposition state, have frequencies directly proportional to the energy differences between these eigenstates. The Fourier amplitudes of the beat components depend (1) on the composition of the superposition state and, hence, on the transition amplitudes for excitation of the various eigenstates and (2) on the transition amplitudes corresponding to the probe transitions.

In the case of purely rotational coherence, quantum beats arise from the coherent excitation of rotational levels belonging to the same vibronic state of a molecule ("rotational quantum beats").[1] An example is given in Fig. 1, which portrays part of the level structure of a symmetric top molecule. The molecule, initially in the rotational state $|J_0K_0M_0\rangle$ of the $|S_0v_0\rangle$ vibronic state, is excited by a linearly polarized (polarization vector $\hat{e}_1$ parallel to the laboratory Z axis), broadband pulse of light to the rotational manifold of the $|S_1v_1\rangle$ vibronic state. Assuming that the $|S_1v_1\rangle \leftarrow |S_0v_0\rangle$ vibronic transition has a parallel-type transition dipole moment, the rotational selection rules $\Delta J = 0, \pm 1$, $\Delta K = 0$, and $\Delta M = 0$ obtain.[10] Therefore, three $|S_1v_1\rangle$ rotational levels (those shown in the figure) are prepared coherently in the excitation process. Assuming, further, that one monitors (with polarization $\hat{e}_2$ parallel to $\hat{e}_1$) the intensity vs time of a parallel-type emission band, comprised of transitions from this $|S_1v_1\rangle$ superposition state to the rotational manifold of some final vibronic state $|S_0v_2\rangle$, then $\Delta J = 0, \pm 1$, $\Delta K = 0$, and $\Delta M = 0$ rotational selection rules characterize the emission process, also. Hence, the three $|S_1v_1\rangle$ rotational eigenstates can collectively emit to a total of five $|S_0v_2\rangle$ rotational

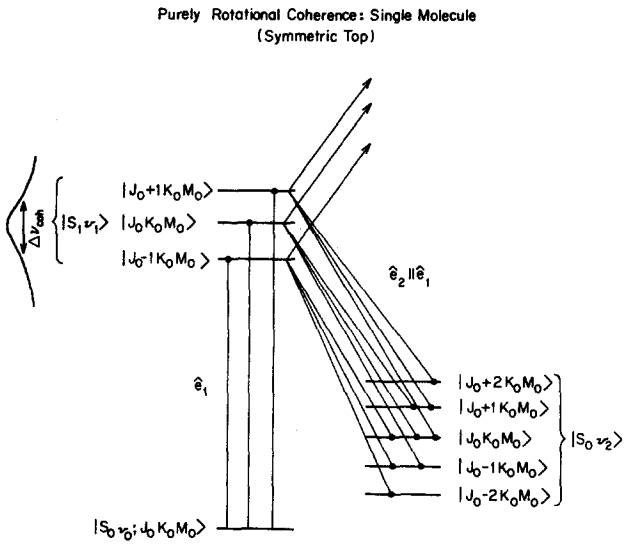

FIG. 1. Level diagram showing the eigenstates associated with rotational quantum beats in the temporally resolved fluorescence of a symmetric top molecule with parallel-type absorption and emission dipole moments. The detection polarization ($\hat{e}_2$) is assumed linear and parallel to the linearly polarized ($\hat{e}_1$) excitation light. $\Delta\nu_{coh}$ denotes the coherence width of the laser excitation source. Absorption transitions occur from a single rovibronic level in a ground vibronic state manifold to the three rotational levels in the excited vibronic state that can combine in absorption with the ground state level. Fluorescence transitions to the final ground vibronic state, because of angular momentum selection rules, can occur to only five rotational levels. Arrows pointing up indicate the possibility of probing the excited superposition state by some means (e.g., absorption or pulsed laser-induced ionization) other than fluorescence.

levels (see Fig. 1). Moreover, each of the three pairs of the prepared $|S_1v_1\rangle$ eigenstates can emit to at least one *common* $|S_0v_2\rangle$ rotational level. Therefore, the situation depicted in Fig. 1 meets the criteria for beat-modulated fluorescence decays. The intensity vs time of the $|S_1v_1\rangle \rightarrow |S_0v_2\rangle$ emission will be modulated by three beat frequencies (rotational quantum beats), corresponding to the energy differences between each of the three distinct pairs of coherently prepared $|S_1v_1\rangle$ eigenstates. The modulation depths of the beat components are determined by the relative values of the probability amplitudes for the nine possible excitation-emission channels.

At this point it is important to point out that excitation and detection polarization play a large role in determining the characteristics of rotational quantum beats. Suppose, for example, that $\hat{e}_2$ is set perpendicular to $\hat{e}_1$ instead of parallel. Then, the emission selection rule on M is $\Delta M = \pm 1$. The set of $|S_0v_2\rangle$ rotational levels pertinent to this polarization case is entirely different from the set pertinent to the $\hat{e}_2\|\hat{e}_1$ case. Since beat modulation depths depend on the probability amplitudes of the possible excitation-emission channels, then clearly the qualitative change in the nature of these channels that occurs upon changing the polarizations in the experiment will lead to a change in beat characteristics. In this regard, excited state rotational quantum beats are analogous to fine structure, hyperfine structure, and Zeeman level quantum interference effects,[3,11–18] and to ground state rotational coherence in nonlinear optical experiments,[19] all effects of which are also polarization dependent. Rotational quantum beats are different, however, from other types of beats in molecules, beats which are polarization independent. Notable examples are the beats that arise from singlet–triplet coupling,[20–24] singlet–singlet coupling,[25] and from IVR.[26]

The case considered in Fig. 1 can be generalized in a number of ways. One can consider asymmetric top molecules. One can treat cases wherein the absorption and emission dipoles are not parallel-type. And/or, one can consider cases wherein the excitation and detection polarizations are arbitrary. *In all these cases rotational quantum beats are possible*, though their characteristics may vary from case to case. Much of what follows in this paper is directed toward determining the characteristics (in particular, the Fourier amplitudes) of rotational quantum beats under a variety of circumstances.

B. Thermal averaging

If it were possible to ensure that each molecule in one's sample was in exactly the same rovibronic state prior to any excitation pulse, then one's consideration of rotational coherence effects would be tantamount to a consideration of rotational quantum beats. However, samples of large molecules, even samples cooled by free jet expansion, are characterized by thermal distributions in which many rotational states have appreciable probabilities of being populated. Thus, there is a broad distribution of initial states in such samples. Now, excitation from different initial rotational states will give rise to different quantum beat-modulated decays. For example, the situation depicted in Fig. 1 is characterized by fluorescence decays with three beat components having frequencies $\nu_1 = 2J_0B$, $\nu_2 = 2(J_0+1)B$, and $\nu_3 = 2(2J_0+1)B$, respectively. (B, in frequency units, is the rotational constant of the molecule for rotation about either of its two identical, principal inertial axes.) Clearly, as J_0 changes, these three frequencies also change. In addition, beat modulation depths vary with J_0 and K_0 (i.e., with the rotational quantum numbers of the initial state). The upshot of all the above is that, *for a sample at finite temperature, an observed decay is the thermally weighted average of many different, beat-modulated decays.*[1]

Now, in general, the summation of many sinusoidal terms having random frequencies and amplitudes (including sign) tends toward a resultant equal to zero at all times. Therefore, one might expect that the thermal averaging of rotational quantum beats would lead to a washing out of the manifestations of rotational coherence. However, this does not occur.[1] The reason for this is that the frequencies and amplitudes of rotational quantum beats do not vary randomly with the rotational quantum numbers of the initial state. In this regard, it is once again illustrative to make reference to the particular situation shown in Fig. 1. It is possible to show[1] that the fluorescence decay corresponding to this case (neglecting any population decay and accounting for the isotropy of the sample by summing over M_0) is of the form

$$I(J_0,K_0,t) = f_0(J_0,K_0) + \sum_{i=1}^{3} f_i(J_0,K_0)\cos 2\pi\nu_i t, \quad (2.1)$$

with the ν_i as given above and where f_0 and the f_i are functions of J_0, and K_0. The thermal average of many such decays is

$$I(t,T) = \sum_{J_0,K_0} P(J_0,K_0,T) \times \left[f_0(J_0,K_0) + \sum_{i=1}^{3} f_i(J_0,K_0)\cos 2\pi\nu_i t \right], \tag{2.2}$$

where T is the temperature, and $P(J_0,K_0,T)$ is the thermal population of $|S_0\nu_0\rangle$ rotational levels having quantum numbers J_0,K_0. Now, the expressions for the ν_i indicate that every cosine term entering into Eq. (2.2) is an integer multiple of $2B$. Moreover, one can show that *each* f_i that appears in the equation, regardless of J_0 and K_0, *is positive* for $\hat{e}_1$ parallel to $\hat{e}_2$. From both of these facts, it is apparent that at times $t = n/(2B)$, $n = 0,1,2,...$, all cosine terms in Eq. (2.2) constructively interfere.[1] At times different from these times, such constructive interference does not occur. (Partial constructive interferences do occur at specific times. This will be discussed in Sec. IV.) Thus, there are periodic recurrences in $I(t,T)$ that are manifestations of the thermal averaging of rotational coherence and that have spacings determined by the B rotational constant of the molecule. Notably, for $\hat{e}_1$ perpendicular to $\hat{e}_2$, recurrences also occur at times identical to the ones in the $\hat{e}_1\|\hat{e}_2$ case, but with opposite polarity. As shown in Secs. IV and V the relation between the magnitude of the transients in the parallel and perpendicular cases is such that in the sum of intensities, $I(\|,t) + 2I(\perp,t)$, the recurrences associated with rotational coherence vanish.

It will be shown in this paper that those characteristics of rotational quantum beats that prevent the thermal washing out of rotational coherence effects in symmetric top molecules with parallel-type absorption and emission dipoles also are present, at least to an approximate degree, in more general situations.

II. THEORETICAL FRAMEWORK

It shall be useful in this paper to have a general framework with which to consider the observable manifestations of rovibrational coherence in molecules. We shall use a density matrix/spherical tensor formalism. The approach closely follows that of Silverman *et al.*[9] in their treatment of atomic quantum beats. We choose this method for a number of reasons:

(1) It is uniquely suited to the description of the angular and polarization properties of observables associated with atomic and molecular species.

(2) It allows, in a very natural and succinct way, for the inclusion of coherence effects arising from *intramolecular couplings*.

(3) It can be extended readily to account for multiphoton excitation and/or probe processes,[9(b)] for the influence that collisions have on rotational coherence effects, and for the possibility of spatially anisotropic samples (Such extensions, however, will not be undertaken in this paper.)

A. Preliminaries

Throughout the remainder of the paper, we shall consider variations on the same general physical situation. We assume that a time domain experiment, consisting of polarized (polarization vector $\hat{e}_1$) pulsed-laser excitation, followed by the measurement in time of polarized (polarization vector $\hat{e}_2$) fluorescence, is performed on a (initially) *spatially isotropic*,[27] thermal sample of isolated molecules. We label the observable $I(t,\hat{e}_1,\hat{e}_2,T)$, indicating its dependences on time, excitation and detection polarization, and the temperature of the sample. We assume that the excitation pulse is sufficiently weak in intensity to allow one to ignore nonlinear intensity effects,[28] and is also of sufficiently short duration to allow one to consider excitation and probe processes as being distinct. Regarding the quantum transitions of individual molecules of the sample in the excitation and fluorescence steps, we assume that they are single photon and are electric dipole induced.

The above situation implies that three parts of the molecular level structure (see Fig. 2), with three associated partial density matrices and projection operators are pertinent to the experiment. One part corresponds to the thermally available states of the molecule, the states populated prior to any excitation pulse. (These will typically be rovibrational states in the ground electronic state of the molecule.) To label these states we use quantum numbers with a subscript "0"—a generic state is given as $|\Gamma_0 M_0\rangle$, where M_0 is the quantum number associated with the projection of the total rotational angular momentum on a spaced-fixed axis, and Γ_0 denotes the set of all other quantum numbers describing the state. (The convenience in separating M quantum numbers from the others will become apparent.) The partial density matrix of the sample, corresponding to molecules in this thermally populated part of the molecular level structure, will be denoted as σ_0, and the projection operator as P_0.

The second relevant part of the level structure corresponds to the rovibronic states populated by the laser pulse. We denote these states, associated partial density matrix, and projection operator, with a subscript "1"—$|\Gamma_1 M_1\rangle$, σ_1, and P_1, respectively.

Finally, the third relevant part of the level structure corresponds to the final states in the fluorescence transitions. These states we denote as $|\Gamma_2 M_2\rangle$, and the projection operator as P_2. (In the experimental scheme considered here there is no need to consider the partial density matrix associated with this manifold.)

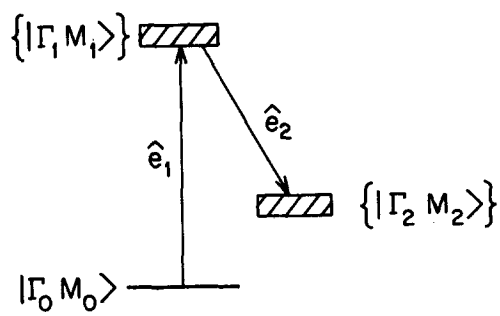

FIG. 2. Level diagram indicating the generic experiment to be considered herein. Pulsed, polarized excitation occurs from a ground electronic state rovibrational level $|\Gamma_0 M_0\rangle$ to the manifold of excited rovibronic states $\{|\Gamma_1 M_1\rangle\}$. Polarized fluorescence from the excited state thereby prepared to the manifold of final ground rovibrational states $\{|\Gamma_2 M_2\rangle\}$ is then detected as a function of time.

B. Expression for the observable $I(t,\hat{e}_1,\hat{e}_2,T)$

The general expression for the observable associated with a sample having density matrix σ and a probe process represented by the operator Θ_{pr} is

$$I = K\,\mathrm{Tr}\{\sigma\Theta_{pr}^{\dagger}\}, \tag{3.1}$$

where all the dependences of I on experimental parameters have been suppressed, Tr represents the trace operation, and K is a constant (which shall henceforth be suppressed). For the dipole pump/dipole probe experiment to be considered herein[9(a)]

$$\Theta_{pr} = P_1(\hat{e}_2\cdot\mathbf{d})P_2(\hat{e}_2\cdot\mathbf{d})^*P_1, \tag{3.2}$$

where $\mathbf{d}$ is the dipole moment operator. This expression implies that σ in Eq. (3.1) can be replaced by the partial density matrix σ_1. σ_1, however, is determined (1) by the effect of the excitation process on the initial density matrix of the sample $[\sigma_0(T)]$ and (2) by the molecular Hamiltonian H, which governs the temporal evolution of σ_1 subsequent to the duration of the excitation pulse:

$$\sigma_1(0^+,\hat{e}_1,T) = P_1(\hat{e}_1\cdot\mathbf{d})P_0\sigma_0(T)P_0(\hat{e}_1\cdot\mathbf{d})^*P_1 \tag{3.3}$$

and

$$\sigma_1(t,\hat{e}_1,T) = e^{-iHt/\hbar}\sigma_1(0^+,\hat{e}_1,T)e^{iHt/\hbar}, \tag{3.4}$$

where $\sigma_1(0^+,\hat{e}_1,T)$ is σ_1 instantaneously after the duration of the excitation pulse, and $\sigma_1(t,\hat{e}_1,T)$ is σ_1 as it evolves in time. Equations (3.2)–(3.4) substituted in Eq. (3.1) give the observable $I(t,\hat{e}_1,\hat{e}_2,T)$.

To proceed further in the analysis of Eqs. (3.1)–(3.4) it is a considerable convenience to express σ_0, σ_1, Θ_{pr}, and the P_i in terms of irreducible tensor operators.[9(b)] Therefore, we define such operators as follows:

$$ {}^{\Gamma_i\Gamma_i'}T^{L_i}_{l_i} \equiv \sum_{M_i,M_i'} (2L_i+1)^{1/2}(-1)^{J_i-M_i} \times \begin{pmatrix} J_i & L_i & J_i' \\ -M_i & l_i & M_i' \end{pmatrix} |\Gamma_i M_i\rangle\langle\Gamma_i' M_i'|, \tag{3.5}$$

where J_i and J_i' are the rotational angular momentum quantum numbers for the states $|\Gamma_i\, M_i\rangle$ and $|\Gamma_i'\, M_i'\rangle$, respectively. {Equation (3.5) represents an extension of Silverman *et al.*'s expression [Eq. (2) of Ref. 9(b)] to account for the vibrational and rotational level structure of molecules.} These operators are characterized by several useful properties.[9(b)] First, they are orthonormal under the trace operation

$$\mathrm{Tr}\{{}^{\Gamma_i\Gamma_i'}T^{L_i}_{l_i} \times ({}^{\Gamma_i''\Gamma_i'''}T^{L_i'}_{l_i'})^{\dagger}\} = \delta_{\Gamma_i,\Gamma_i''}\delta_{\Gamma_i',\Gamma_i'''}\delta_{L_i,L_i'}\delta_{l_i,l_i'}. \tag{3.6}$$

Second, upon rotation through the Euler angles[29] $(\alpha,\beta,\gamma)\equiv\Omega$, they transform as

$$D(\Omega)({}^{\Gamma_i\Gamma_i'}T^{L_i}_{l_i})D^{-1}(\Omega) = \sum_{l_i'} D^{(L_i)}_{l_i'l_i}(\Omega) \times {}^{\Gamma_i\Gamma_i'}T^{L_i}_{l_i'}, \tag{3.7}$$

where $D^{(L_i)}_{l_i'l_i}$ is an element of the Wigner rotation matrix. Finally, they evolve in time in a manner analogous to σ_1 [Eq. (3.4)]. In the particular case where one chooses the basis states $|\Gamma_i M_i\rangle$ to be eigenstates of the molecular Hamiltonian, the temporal evolution is given by

$$e^{-iHt/\hbar}({}^{\Gamma_i\Gamma_i'}T^{L_i}_{l_i})e^{iHt/\hbar} = {}^{\Gamma_i\Gamma_i'}T^{L_i}_{l_i} \times e^{-i\omega_{\Gamma_i\Gamma_i'}t}e^{-\gamma t}, \tag{3.8}$$

where $\omega_{\Gamma_i\Gamma_i'} = (E_{\Gamma_i} - E_{\Gamma_i'})/\hbar$, E_{Γ_i} and $E_{\Gamma_i'}$ are the energies of $|\Gamma_i M_i\rangle$ and $|\Gamma_i' M_i'\rangle$, respectively, and γ is a constant that accounts for the decay of the states.[31]

One can now express the partial density matrices as linear combinations of the tensor operators:

$$\sigma_i = \sum_{\Gamma_i\Gamma_i'}\sum_{L_il_i} \alpha^{\Gamma_i\Gamma_i'}_{L_il_i} \times {}^{\Gamma_i\Gamma_i'}T^{L_i}_{l_i} \tag{3.9}$$

with the α's given by

$$\alpha^{\Gamma_i\Gamma_i'}_{L_il_i'} = \mathrm{Tr}\{\sigma_i \times ({}^{\Gamma_i\Gamma_i'}T^{L_i}_{l_i})^{\dagger}\}. \tag{3.10}$$

One can also express Θ_{pr} and the projection operators in analogous ways:

$$\Theta_{pr} = \sum \beta^{\Gamma_1\Gamma_1'}_{L_1l_1} \times {}^{\Gamma_1\Gamma_1'}T^{L_1}_{l_1} \tag{3.11}$$

and

$$P_i = \sum \phi^{\Gamma_i\Gamma_i'}_{L_il_i} \times {}^{\Gamma_i\Gamma_i'}T^{L_i}_{l_i}. \tag{3.12}$$

Now, following Silverman *et al.*,[9(b)] we note that Eq. (3.3) implies a linear relation of the following form between the α coefficients for σ_0 and for $\sigma_1(0^+)$:

$$\alpha^{\Gamma_1\Gamma_1'}_{L_1l_1} = \sum \left[{}^{\Gamma_1\Gamma_1'}_{L_1l_1}A^{\Gamma_0\Gamma_0'}_{L_0l_0}(\hat{e}_1)\right] \times \alpha^{\Gamma_0\Gamma_0'}_{L_0l_0}, \tag{3.13}$$

where the sum is over repeated indices. Similarly, the β's and ϕ's in Eqs. (3.11) and (3.12) are also related by a linear transformation

$$\beta^{\Gamma_1\Gamma_1'}_{L_1l_1} = \sum \left[{}^{\Gamma_1\Gamma_1'}_{L_1l_1}A^{\Gamma_2\Gamma_2'}_{L_2l_2}(\hat{e}_2)\right] \times \phi^{\Gamma_2\Gamma_2'}_{L_2l_2}. \tag{3.14}$$

Furthermore, because Eqs. (3.2) and (3.3) have the same form [P_2 is to Θ_{pr} as σ_0 is to $\sigma_1(0^+)$], the A coefficients in Eqs. (3.13) and (3.14) are given by the same equation[9(b)]:

$$\begin{aligned} {}^{\Gamma_i\Gamma_i'}_{L_il_i}A^{\Gamma_k\Gamma_k'}_{L_kl_k}(\hat{e}) &= \mathrm{Tr}\{P_i(\hat{e}\cdot\mathbf{d})P_k({}^{\Gamma_k\Gamma_k'}T^{L_k}_{l_k})P_k(\hat{e}\cdot\mathbf{d})^*P_i({}^{\Gamma_i\Gamma_i'}T^{L_i}_{l_i})^{\dagger}\} \\ &= (-1)^{J_i+J_k}(2L_i+1)^{1/2}(2L_k+1)^{1/2} \\ &\times \sum_{M_i,M_i'}\sum_{M_k,M_k'} (-1)^{M_i+M_k} \begin{pmatrix} J_i & L_i & J_i' \\ -M_i & l_i & M_i' \end{pmatrix} \begin{pmatrix} J_k & L_k & J_k' \\ -M_k & l_k & M_k' \end{pmatrix} \\ &\times \langle\Gamma_i M_i|\hat{e}\cdot\mathbf{d}|\Gamma_k M_k\rangle\langle\Gamma_k' M_k'|(\hat{e}\cdot\mathbf{d})^*|\Gamma_i' M_i'\rangle, \end{aligned} \tag{3.15}$$

where $|i-k|=1$. Note that since $\mathbf{d}$ is real, the following holds:

$$\left[{}^{\Gamma_i\Gamma_i'}_{L_iI_i}A^{\Gamma_k\Gamma_k'}_{L_kI_k}(\hat{e})\right]^* = {}^{\Gamma_k\Gamma_k'}_{L_kI_k}A^{\Gamma_i\Gamma_i'}_{L_iI_i}(\hat{e}^*). \tag{3.16}$$

The utility of Eqs. (3.13)–(3.16) resides primarily in the fact that they allow a very convenient expression of the polarization dependences of $I(t,\hat{e}_1,\hat{e}_2,T)$. To see this, note that for a thermal, isotropic[27] sample

$$\alpha^{\Gamma_0\Gamma_0'}_{L_0I_0} = (\delta_{\Gamma_0,\Gamma_0'})(\delta_{L_0,0})(\delta_{I_0,0})\times(2J_0+1)^{1/2} \times\frac{G(\Gamma_0)e^{-E_{\Gamma_0}/k_BT}}{Q}, \tag{3.17}$$

where Q is the partition function of the sample, $G(\Gamma_0)$ is the nuclear spin statistical weight of $|\Gamma_0M_0\rangle$, and k_B is Boltzmann's constant. Note also that

$$\phi^{\Gamma_2\Gamma_2'}_{L_2I_2} = (\delta_{\Gamma_2,\Gamma_2'})(\delta_{L_2,0})(\delta_{I_2,0})\times(2J_2+1)^{1/2}. \tag{3.18}$$

By using Eqs. (3.17) and (3.18) in Eqs. (3.13) and (3.14), and then substituting the latter two equations along with Eqs. (3.9) and (3.11) into Eqs. (3.1)–(3.4), one obtains the following general expression for the observable:

$$\begin{aligned} I(t,\hat{e}_1,\hat{e}_2,T) = \sum {}^{\Gamma_i\Gamma_i'}_{L_iI_i}A^{\Gamma_0\Gamma_0}_{00}(\hat{e}_1)\left[{}^{\Gamma_1''\Gamma_1'''}_{L_1'I_1'}A^{\Gamma_2\Gamma_2}_{00}(\hat{e}_2)\right]^* \\ \times(2J_2+1)^{1/2}(2J_0+1)^{1/2} \\ \times\frac{G(\Gamma_0)e^{-E_{\Gamma_0}/k_BT}}{Q}\,\mathrm{Tr}\{e^{-iHt/\hbar}({}^{\Gamma_1\Gamma_i'}T^{L_i'}_{I_i}) \\ \times e^{iHt/\hbar}({}^{\Gamma_1''\Gamma_1'''}T^{L_1'}_{I_1'})^\dagger\}, \end{aligned} \tag{3.19}$$

where the summation is over all the Γ's, L's, and l's, and where the A's are given by Eq. (3.15). In the cases where one chooses the basis states $|\Gamma_iM_i\rangle$ as eigenstates of H, Eq. (3.19) becomes

$$\begin{aligned} I(t,\hat{e}_1,\hat{e}_2,T) = \sum {}^{\Gamma_i\Gamma_i'}_{L_iI_i}A^{\Gamma_0\Gamma_0}_{00}(\hat{e}_1)\left[{}^{\Gamma_i\Gamma_i'}_{L_iI_i}A^{\Gamma_2\Gamma_2}_{00}(\hat{e}_2)\right]^* \\ \times(2J_2+1)^{1/2}(2J_0+1)^{1/2} \\ \times\frac{G(\Gamma_0)e^{-E_{\Gamma_0}/k_BT}}{Q}e^{-i\omega_{\Gamma_i\Gamma_i'}t}e^{-\gamma t}. \end{aligned} \tag{3.20}$$

From Eq. (3.19) or (3.20) *it is evident that all the polarization dependence of the observable is contained in the A factors.* This is very convenient because the rotational transformation properties of these factors[9(b)] introduce considerable simplification into their evaluation for arbitrary linear or circular polarizations. In particular, one need only evaluate the $A(\hat{e})$ [Eq. (3.15)] for the three principal[9(b)] polarizations $e^{1,Q}, Q=0,\pm1$, where the $e^{1,Q}$ are the usual spherical unit vector components[30]: $e^{1,0}=\hat{e}_Z$, $e^{1,1}=-2^{-1/2}(\hat{e}_X+i\hat{e}_Y)$, and $e^{1,-1}=2^{-1/2}(\hat{e}_X-i\hat{e}_Y)$. For polarizations other than principal ones, the $A(\hat{e})$ can be found by the rotational transformation relations[32]

$${}^{\Gamma_i\Gamma_i'}_{L_iI_i}A^{\Gamma_k\Gamma_k}_{00}(\hat{e}_i) = D^{(L_i)}_{I\rho}(\phi,\theta,0)\,{}^{\Gamma_i\Gamma_i'}_{L\rho}A^{\Gamma_k\Gamma_k}_{00}(Q_i), \tag{3.21}$$

where ϕ and θ are the Euler angles describing the orientation of the polarization axis of $\hat{e}_i$ with respect to the laboratory Z axis, and where the $A(Q_i)$ are the A factors for the appropriate principal polarizations ($Q_i=0,\pm1$ for linear, right-hand circular, and left-hand circular polarizations, respectively). In this paper, we shall choose the laboratory Z axis to be along the polarization axis of $\hat{e}_2$. Therefore, we will need to consider transformations of ${}^{\Gamma_i\Gamma_i'}_{L_iI_i}A^{\Gamma_0\Gamma_0}_{00}(Q_1)$, only.

Equations (3.19) and (3.20) represent the main results of this section. Equation (3.20), which gives the observable (for an initially isotropic sample) when the $|\Gamma_1M_1\rangle$ are taken as eigenstates of the molecule, will be applied to the consideration of purely rotational coherence (Secs. IV and V). The more general equation (3.19) will be used to treat problems in which both rotational coherence and intramolecular couplings contribute to interference effects in $I(t,\hat{e}_1,\hat{e}_2,T)$ (Sec. VIII).

IV. Purely rotational coherence in symmetric top molecules

We shall apply now the formalism presented in the previous section to the case of purely rotational coherence effects in the fluorescence decays of symmetric top molecules. The physical situation we consider is illustrated in Fig. 3. We assume that only three singlet *vibronic* levels are involved: (1) one initial level, the only vibronic level populated thermally in the sample; (2) one excited state level, the only one connected to the initial level via the laser; and (3) a final ground vibrational state, corresponding to the particular band in the emission spectrum that we have decided to detect (by tuning a monochromator, for example). These three levels we label, respectively, $|S_0v_0\rangle$, $|S_1v_1\rangle$, and $|S_0v_2\rangle$, where S_0 and S_1 denote the ground and excited electronic states, and the v's denote the three vibrational levels. We assume that the excitation and detection conditions are such that all the rotational levels of the $|S_1v_1\rangle$ and $|S_0v_2\rangle$ manifolds are pertinent. Hence, the states in the problem are $|\Gamma_0M_0\rangle = |S_0v_0;J_0K_0M_0\rangle$, $|\Gamma_1M_1\rangle = |S_1v_1;J_1K_1M_1\rangle$, and $|\Gamma_2M_2\rangle = |S_0v_2;J_2K_2M_2\rangle$, where the J's, K's, and M's are the usual symmetric top quantum numbers. All these states are taken to be eigenstates of H. Therefore, to calculate the observable signal for an initially isotropic sample we use Eq. (3.20). Summations of the form Σ_{Γ_i} in this equation become $\Sigma_{J_iK_i}$ since all rotational levels are pertinent and the vibronic quantum numbers are fixed.

Using symmetric top eigenfunctions in Eq. (3.15) yields the expression

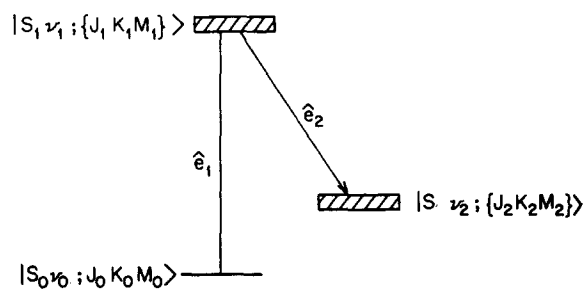

$$
\begin{aligned}
{}^{\Gamma_i\Gamma_i'}_{L_iI_i}A^{\Gamma_k\Gamma_k'}_{L_kI_k}(Q_i) = \delta_{I_i,I_k}\sum_{q_iq_i'}\sum_{j}(-1)^{J_i+J_i'+K_i+K_k'}\mu_i^{1,q_i}\mu_i^{1,-q_i'}(2j+1) \\
\times[(2L_i+1)(2L_k+1)(2J_i+1)(2J_k+1)(2J_i'+1)(2J_k'+1)]^{1/2} \\
\times\begin{pmatrix} j & L_k & 1 \\ Q_i-I_k & I_k & -Q_i\end{pmatrix}\begin{pmatrix} j & 1 & L_i \\ Q_i-I_i & -Q_i & I_i\end{pmatrix}\begin{Bmatrix} j & L_k & 1 \\ J_k & J_i & J_k'\end{Bmatrix} \\
\times\begin{Bmatrix} j & 1 & L_i \\ J_i' & J_i & J_k'\end{Bmatrix}\begin{pmatrix} J_i & 1 & J_k \\ -K_i & q_i & K_k\end{pmatrix}\begin{pmatrix} J_k' & 1 & J_i' \\ -K_k' & -q_i' & K_i'\end{pmatrix},
\end{aligned}
\tag{4.1}
$$

where $Q_i = 0, \pm 1$ depending on whether the principal polarization is linear, right-hand circularly polarized, or left-hand circularly polarized, and the usual notation[30] for 3-j and 6-j symbols is used. To obtain Eq. (4.1) from Eq. (3.15) we have assumed the separability of rotational and vibronic coordinates, have transformed $\mathbf{d}$ from the laboratory frame to a spherical vector operator μ^{1,q_i}, $q_i = 0, \pm 1$ in the molecular frame, and have defined μ_i^{1,q_i} as the dipole matrix element:

$$
\mu_i^{1,q_i} \equiv \langle S_i v_i | \mu^{1,q_i} | S_k v_k \rangle. \tag{4.2}
$$

Further, we used Eq. (4.6.2) of Ref. 30 to evaluate the integrals over rotational coordinates and then used Eq. (6.2.8) of the same reference to evaluate the sums over the M quantum numbers.

For the problem at hand, by Eq. (3.20), only two forms of the A coefficients need to be considered: ${}^{\Gamma_i\Gamma_i'}_{L_iI_i}A^{\Gamma_0\Gamma_0}_{00}(Q_1)$ and ${}^{\Gamma_i\Gamma_i'}_{L_iI_i}A^{\Gamma_2\Gamma_2}_{00}(Q_2)$. For ${}^{\Gamma_i\Gamma_i'}_{L_iI_i}A^{\Gamma_0\Gamma_0}_{00}(Q_1)$ the 3-j symbols are nonzero in Eq. (4.1) only if $I_1 = I_0 = 0$, $J_0 = J_0'$, $K_0 = K_0'$, and $j = 1$. Using these facts, one can reduce Eq. (4.1) to

$$
\begin{aligned}
{}^{\Gamma_1\Gamma_1'}_{L_1I_1}A^{\Gamma_0\Gamma_0}_{00}(Q_1) = \delta_{I_1,0}\sum_{q_1q_1'}(-1)^{J_0+J_1'+K_1+K_0+Q_1}\begin{pmatrix} 1 & 1 & L_1 \\ Q_1 & -Q_1 & 0\end{pmatrix} \\
\times[(2L_1+1)(2J_0+1)(2J_1+1)(2J_1'+1)]^{1/2}\mu_1^{1,q_1}\mu_1^{1,-q_1'} \\
\times\begin{Bmatrix} 1 & 1 & L_1 \\ J_1' & J_1 & J_0\end{Bmatrix}\begin{pmatrix} J_1 & 1 & J_0 \\ -K_1 & q_1 & K_0\end{pmatrix}\begin{pmatrix} J_0 & 1 & J_1' \\ -K_0 & -q_1' & K_1'\end{pmatrix}.
\end{aligned}
\tag{4.3}
$$

[To obtain ${}^{\Gamma_i\Gamma_i'}_{L_iI_i}A^{\Gamma_0\Gamma_0}_{00}(\hat{e}_1)$, one uses Eqs. (4.3) and (3.21).] Similar simplifications of Eq. (4.1) apply to $\left[{}^{\Gamma_1\Gamma_1'}_{L_1I_1}A^{\Gamma_2\Gamma_2}_{00}(Q_2)\right]^* = {}^{\Gamma_2\Gamma_2}_{00}A^{\Gamma_1\Gamma_1'}_{L_1I_1}(-Q_2)$. Moreover, one can further simplify things by performing the sum over Γ_2 that appears in Eq. (3.20) to obtain

$$
\begin{aligned}
\sum_{\Gamma_2}(2J_2+1)^{1/2}\left[{}^{\Gamma_2\Gamma_2}_{00}A^{\Gamma_1\Gamma_1'}_{L_1I_1}(-Q_2)\right] = \delta_{I_1,0}\sum_{q_2q_2'}(-1)^{J_1+K_1+L_1+Q_2}\mu_2^{1,q_2}\mu_2^{1,-q_2'} \\
\times[(2L_1+1)(2J_1+1)(2J_1'+1)]^{1/2}\begin{pmatrix} 1 & 1 & L_1 \\ Q_2 & -Q_2 & 0\end{pmatrix} \\
\times\begin{pmatrix} L_1 & 1 & 1 \\ K_1-K_1' & -q_2' & q_2\end{pmatrix}\begin{pmatrix} J_1 & J_1' & L_1 \\ K_1 & -K_1' & K_1'-K_1\end{pmatrix}.
\end{aligned}
\tag{4.4}
$$

Finally, combining Eqs. (4.3), (4.4), (3.20), and (3.21), one obtains

$$
\begin{aligned}
I(t,\hat{e}_1,\hat{e}_2,T) = \sum_{\Gamma_0}\frac{G(\Gamma_0)e^{-E_{\Gamma_0}/k_BT}}{Q}\Bigg[\sum_{\Gamma_1\Gamma_1'}\sum_{q_1q_1'}\sum_{q_2q_2'}\sum_{L_1}(-1)^{J_0+J_1+J_1'+K_0+L_1+Q_1+Q_2} \\
\times D_{00}^{(L_1)}(\phi,\theta,0)(2J_0+1)(2J_1+1)(2J_1'+1)(2L_1+1) \\
\times\mu_1^{1,q_1}\mu_1^{1,-q_1'}\mu_2^{1,q_2}\mu_2^{1,-q_2'}\begin{pmatrix} 1 & 1 & L_1 \\ Q_1 & -Q_1 & 0\end{pmatrix}\begin{pmatrix} 1 & 1 & L_1 \\ Q_2 & -Q_2 & 0\end{pmatrix} \\
\times\begin{pmatrix} L_1 & 1 & 1 \\ q_2'-q_2 & -q_2' & q_2\end{pmatrix}\begin{pmatrix} J_1 & 1 & J_0 \\ -K_1 & q_1 & K_0\end{pmatrix}\begin{pmatrix} J_0 & 1 & J_1' \\ -K_0 & -q_1' & K_1'\end{pmatrix} \\
\times\begin{pmatrix} J_1 & J_1' & L_1 \\ K_1 & -K_1' & q_2-q_2'\end{pmatrix}\begin{Bmatrix} J_1' & J_1 & L_1 \\ 1 & 1 & J_0\end{Bmatrix}e^{-i\omega_{\Gamma_1\Gamma_1'}t}e^{-\gamma t}\Bigg].
\end{aligned}
\tag{4.5}
$$

[We reiterate the fact that the polarization axis of $\hat{e}_2$ defines the laboratory Z axis, so that the $D_{00}^{(L_1)}(\phi,\theta,0)$ factor that appears in Eq. (4.5) pertains to the orientation of the polarization axis of $\hat{e}_1$ with respect to that of $\hat{e}_2$.]

Equation (4.5) is a *general expression for the manifestations, in temporally and spectrally resolved fluorescence, of purely rotational coherence in thermal samples of symmetric top molecules; it is composed of terms which decay monotonically* (those terms for which $\Gamma_1 = \Gamma_1'$) and *terms which modulate the decay* (terms for which $\Gamma_1 \neq \Gamma_1'$, quantum beat terms). We shall examine this equation in more detail in what follows.

A. General results

Without recourse to specific cases of Eq. (4.5) one can derive a number of general results. First, the 3-j symbols give some restrictions on the parameters in the equation. There are the well known selection rules on J and K: $J_1, J_1' = J_0$ or $J_0 \pm 1$, and $K_1 = K_0 + q_1$, $K_1' = K_0 + q_1'$ $(q_1, q_1' = 0, \pm 1)$. The restrictions on the K_1's in turn give $q_2' = q_2 + q_1 - q_1'$. Also, we note that terms in Eq. (4.5) are zero unless $L_1 = 0$, 1, or 2, and that if either Q_1 or Q_2 is zero (corresponding to linear polarization in excitation or detection, respectively), then the $L_1 = 1$ terms are zero, too.

An important result can be derived by considering Eq. (4.5) in the form

$$I(t,\hat{e}_1,\hat{e}_2,T) = C \sum_{\Gamma_0} \frac{G(\Gamma_0) e^{-E_{\Gamma_0}/k_B T}}{Q} \times \sum_{\Gamma_1,\Gamma_1'} f(J_0,J_1,J_1',K_0,K_1,K_1') e^{-i\omega_{\Gamma_1\Gamma_1'} t} e^{-\gamma t}, \tag{4.6}$$

where C is a constant. From the properties of the 3-j and 6-j symbols in Eq. (4.5), one can prove that the f's are real and that

$$f(J_0,J_1,J_1',K_0,K_1,K_1') = f(J_0,J_1',J_1,K_0,K_1',K_1) \tag{4.7}$$

if both μ_1 and μ_2 lie along principal axes of the molecule. In such cases, $I(t,\hat{e}_1,\hat{e}_2,T)$ is temporally modulated solely by cosine terms.

Third, we note that if $L_1 = 0$, then only terms having $J_1 = J_1'$ and $K_1 = K_1'$ are nonzero. Therefore, all modulation terms in the equation (terms which correspond to nonzero $\omega_{\Gamma_1\Gamma_1'}$'s) are associated with $L_1 = 1,2$.

Fourth, assuming linear polarizations, a general relation for the f's in Eq. (4.6) can be proved. For $L_1 = 2$ (which corresponds to all modulation terms for the case of linear polarization) and $\hat{e}_1 \| \hat{e}_2$, $D_{00}^{(2)}(\Omega) = 1$, while for $\hat{e}_1 \perp \hat{e}_2$, $D_{00}^{(2)}(\Omega) = -1/2$. Therefore, for all $L_1 = 2$ terms

$$f_\perp(J_0,J_1,J_1',K_0,K_1,K_1') = -\tfrac{1}{2} f_\parallel(J_0,J_1,J_1',K_0,K_1,K_1'), \tag{4.8}$$

where the subscripts $\perp$ and $\|$ refer to the orientation of $\hat{e}_1$ with respect to $\hat{e}_2$. This result, which is the same as that obtained in the cases of fine structure, hyperfine structure, and Zeeman quantum beats in atoms,[3,11-18] is equivalent to saying that (1) a given beat modulation will have opposite phases for parallel vs perpendicular detection polarization and (2) the total fluorescence of the molecule [proportional to $I(\|) + 2I(\perp)$] is unmodulated in time. Similarly, setting the detection polarizer to the magic angle (54.7° from the parallel direction) will completely eliminate rotational coherence effects in the fluorescence decays, since $D_{00}^{(2)}(\Omega) = 0$ for Ω corresponding to the magic angle. This is analogous to eliminating rotational anisotropy effects in solution phase fluorescence experiments by analyzing the fluorescence at the magic angle.[33]

Another property which has been associated with fluorescence anisotropy in solution is the value of the anisotropy at $t = 0$:

$$r(0) \equiv \frac{I(\|) - I(\perp)}{I(\|) + 2I(\perp)}. \tag{4.9}$$

For molecules in solution with transition dipoles along principal diffusion axes, $r(0)$ equals 0.4 if the absorption and emission dipoles are parallel to each other and equals -0.2 if these dipoles are perpendicular to each other.[33(a)] One can show [either using the general equation (4.5), or the results of Tables I and II, which results will be discussed in the next subsection] that an analogous situation obtains for freely rotating, symmetric top molecules: with μ_1 and μ_2 along principal rotation axes of the molecule and parallel to each other, $r(0) = 0.4$, while with the dipoles along principal rotation axes and perpendicular, $r(0) = -0.2$. [One suspects that these values for $r(0)$ might also obtain when μ_1 and μ_2 do not lie along principal rotational axes. This, we have not proved, however.]

B. Specific cases

Equation (4.5) [or its equivalent, Eq. (4.6)] is general in the sense that it allows for any possible orientation of absorption and emission dipoles and any orientation of excitation and detection polarizations. It is possible to obtain explicit expressions for the terms in Eq. (4.5) if one assumes a specific set of orientations for the dipole vectors and the polarization vectors. We present in this section such results for eight important cases of the equation: when $\hat{e}_1$ and $\hat{e}_2$ are linear polarizations and are either parallel or perpendicular to each other, and when the directions of the absorption and emission transition dipoles relative to the molecule's symmetry axis are either $(\|,\|)$, $(\|,\perp)$, $(\perp,\|)$, or $(\perp,\perp)$. (The notation is such that, for example, $(\|,\perp)$ corresponds to parallel-type absorption and perpendicular-type emission dipole moments.)

Expressions for the f's of Eq. (4.6), determined using Eq. (4.5) and standard tables of 3-j and 6-j symbols[30] are given for the $(\|,\|)$ and $(\|,\perp)$ cases in Table I, and for the $(\perp,\|)$ and $(\perp,\perp)$ dipole cases in Table II. Regarding Table I one would note that the parallel absorption selection rules permit the preparation of only three excited state rotational levels from any given ground state level. Thus, for the $(\|,\|)$ and $(\|,\perp)$ cases there are three beat frequencies per initial state. (These are given in Table I.) One would also note that the factors for the $(\|,\|)$ case with $\hat{e}_1 \perp \hat{e}_2$ are equal to those for the $(\|,\perp)$ case with $\hat{e}_1 \| \hat{e}_2$. This result points up the general fact that detecting different fluorescence band types (i.e., bands with different emisison dipole directions) will give

TABLE I. f values of a symmetric top for ||,|| dipole directions[a] and for ||,⊥ dipole directions.[b]

J_1	J_1'	$K_1 = K_1'$	$f(J_0,J_1,J_1',K_0) = f(J_0,J_1',J_1,K_0)$	$\omega/2\pi$
J_0-1	J_0-1	K_0	$\frac{(J_0^2-K_0^2)}{J_0}\left[-\frac{U(\hat{e}_f)[3K_0^2-J_0(J_0-1)]}{45J_0(2J_0+1)}+\frac{1}{9}\right]$	0
J_0	J_0	K_0	$\frac{(2J_0+1)K_0^2}{J_0(J_0+1)}\left[\frac{U(\hat{e}_f)[3K_0^2-J_0(J_0+1)]}{45J_0(J_0+1)}+\frac{1}{9}\right]$	0
J_0+1	J_0+1	K_0	$\frac{(J_0+1)^2-K_0^2}{(J_0+1)}\left[-\frac{U(\hat{e}_f)[3K_0^2-(J_0+1)(J_0+2)]}{45(J_0+1)(2J_0+1)}+\frac{1}{9}\right]$	0
J_0	J_0-1	K_0	$\frac{U(\hat{e}_f)K_0^2(J_0^2-K_0^2)}{15(J_0+1)J_0^2}$	$2BJ_0$
J_0+1	J_0-1	K_0	$\frac{U(\hat{e}_f)[(J_0+1)^2-K_0^2](J_0^2-K_0^2)}{15J_0(J_0+1)(2J_0+1)}$	$2B(2J_0+1)$
J_0+1	J_0	K_0	$\frac{U(\hat{e}_f)[(J_0+1)^2-K_0^2]K_0^2}{15J_0(J_0+1)^2}$	$2B(J_0+1)$

[a] For ||,|| dipoles $U(\hat{e}_f)=2$ for parallel detection polarization and $U(\hat{e}_f)=-1$ for perpendicular detection polarization.
[b] For ||,⊥ dipoles $U(\hat{e}_f)=-1$ for parallel detection polarization and $U(\hat{e}_f)=1/2$ for perpendicular detection polarization.

rise to different results in a fluorescence polarization experiment. Similarly, if one detects total fluorescence (no rotational or *vibrational* structure resolved), one must know the relative intensities of the various band types in the fluorescence spectrum if one wishes to make an accurate interpretation of observed polarization behavior (whether in a time domain or steady-state experiment).

Referring to Table II, one finds that for the (⊥,||) case, the only nonzero f's are those corresponding to $K_1 = K_1'$. This does not arise from the pependicular-type absorption

TABLE II. f values of a symmetric top for ⊥,|| dipole directions[a] and for ⊥,⊥ dipole directions.[b]

J_1	J_1'	K_1	K_1'	$f(J_0,J_1,J_1',K_0,K_1,K_1') = f(J_0,J_1',J_1,K_0,K_1',K_1)$	$\omega/2\pi$
J_0-1	J_0-1	$K_0\pm1$	$K_0\pm1$	$\frac{(J_0\mp K_0-1)(J_0\mp K_0)}{4J_0}\left[-\frac{U(\hat{e}_f)[3(K_0\pm1)^2-J_0(J_0-1)]}{45J_0(2J_0+1)}+\frac{1}{9}\right]$	0
J_0	J_0	$K_0\pm1$	$K_0\pm1$	$\frac{(2J_0+1)(J_0\pm K_0+1)(J_0\mp K_0)}{4J_0(J_0+1)}\left[\frac{U(\hat{e}_f)[3(K_0\pm1)^2-J_0(J_0+1)]}{45J_0(J_0+1)}+\frac{1}{9}\right]$	0
J_0+1	J_0+1	$K_0\pm1$	$K_0\pm1$	$\frac{(J_0\pm K_0+1)(J_0\pm K_0+2)}{4(J_0+1)}\left[-\frac{U(\hat{e}_f)[3(K_0\pm1)^2-(J_0+1)(J_0+2)]}{45(J_0+1)(2J_0+1)}+\frac{1}{9}\right]$	0
J_0	J_0-1	$K_0\pm1$	$K_0\pm1$	$\frac{U(\hat{e}_f)(1\pm K_0)[J_0^2-(K_0\pm1)^2](J_0\mp K_0)}{60(J_0+1)J_0^2}$	$2BJ_0$
J_0+1	J_0-1	$K_0\pm1$	$K_0\pm1$	$-\frac{U(\hat{e}_f)[J_0^2-(K_0\pm1)^2](J_0\pm K_0+2)(J_0\mp K_0)}{60J_0(J_0+1)(2J_0+1)}$	$2B(2J_0+1)$
J_0+1	J_0	$K_0\pm1$	$K_0\pm1$	$-\frac{U(\hat{e}_f)(J_0\pm K_0+1)(J_0\pm K_0+2)(J_0\mp K_0)(1\pm K_0)}{60J_0(J_0+1)^2}$	$2B(J_0+1)$
J_0-1	J_0-1	K_0+1	K_0-1	$\frac{V(\hat{e}_f)(J_0+K_0-1)(J_0-K_0-1)(J_0^2-K_0^2)}{240J_0^2(2J_0+1)}$	$4(A-B)K_0$
J_0	J_0	K_0+1	K_0-1	$\frac{V(\hat{e}_f)(2J_0+1)[(J_0+1)^2-K_0^2](J_0^2-K_0^2)}{240J_0^2(J_0+1)^2}$	$4(A-B)K_0$
J_0+1	J_0+1	K_0+1	K_0-1	$\frac{V(\hat{e}_f)[(J_0+1)^2-K_0^2][(J_0+2)^2-K_0^2]}{240(J_0+1)^2(2J_0+1)}$	$4(A-B)K_0$
J_0	J_0-1	$K_0\mp1$	$K_0\pm1$	$\frac{V(\hat{e}_f)(J_0\mp K_0+1)(J_0\pm K_0)(J_0\mp K_0-1)(J_0\mp K_0)}{240J_0^2(J_0+1)}$	$2BJ_0\mp4(A-B)K_0$
J_0+1	J_0-1	$K_0\mp1$	$K_0\pm1$	$\frac{V(\hat{e}_f)(J_0\mp K_0+1)(J_0\mp K_0)(J_0\mp K_0-1)(J_0\mp K_0+2)}{240J_0(J_0+1)(2J_0+1)}$	$2B(2J_0+1)\mp4(A-B)K_0$
J_0+1	J_0	$K_0\mp1$	$K_0\pm1$	$\frac{V(\hat{e}_f)(J_0\mp K_0)(J_0\mp K_0+2)[(J_0+1)^2-K_0^2]}{240J_0(J_0+1)^2}$	$2B(J_0+1)\mp4(A-B)K_0$

[a] For ⊥,|| dipoles $U(\hat{e}_f)=2$ for parallel detection polarization and $U(\hat{e}_f)=-1$ for perpendicular detection polarization, $V(\hat{e}_f)$ always equals zero.
[b] For ⊥,⊥ dipoles $U(\hat{e}_f)=-1$ for parallel detection polarization and $U(\hat{e}_f)=1/2$ for perpendicular detection polarization, $V(\hat{e}_f)=2$ for parallel detection polarization and $V(\hat{e}_f)=-1$ for perpendicular detection polarization.

selection rules, but from the fact that the parallel-type dipole selection rules in emission prohibit two excited state rotational levels with different K's from emitting to the same ground state rotational level. Thus, although the $(\perp,\|)$ case in general allows for the excitation of six excited state rotational levels from a single ground state level, there are not 15 beat frequencies, but six. Furthermore, (1) several of these frequencies are identical, so that there are only three unique frequencies, and (2) the frequencies are the same as in the $(\|,\|)$ and $(\|,\perp)$ cases. In contrast, all 15 beat frequencies arising from the coherent preparation of six levels can occur in the $(\perp,\perp)$ case. Again, several of these frequencies are identical, so that in actual fact there are only ten unique frequencies.

Finally, those terms in Tables I and II for which $\omega_{\Gamma_i\Gamma_i'}$ is zero should correspond to intensity factors in steady-state fluorescence. One can check to see that they do by referring to results in the paper by Loge and Parmenter.[34] In doing this, it must be remembered that our results correspond to detection of all lines in the emission rotational band contour, whereas Loge and Parmenter treat fully resolved emission. One must sum their results over all possible fluorescence transitions to obtain our results. We have performed this algebra and find that our results do check against those of Ref. 34.

C. Numerical simulations

In order to provide examples of the types of fluorescence decays one might expect to observe in a polarization experiment on a real sample of symmetric top molecules at finite temperature, we have numerically simulated decays using Eqs. (4.5) and (4.6), and the results of Tables I and II. This was accomplished using a FORTRAN program run on a VAX-780.

1. Parameters and approximations

Several reasonable approximations were made in the calculations. First, we typically truncated the sums over Γ_0 in Eq. (4.5) at $J_0^{\max} = 500$, $K_0 = -500$ to 500. Whether this is a good approximation or not depends on the rotational constants of the molecule in question and on the temperature. In the cases which we treat herein, $J_0^{\max}$ is more than large enough to be a very good approximation.

A second approximation we made was to account only for the beat modulations below a maximum beat frequency ($\nu_{\max}$). The Fourier amplitudes of frequencies greater than $\nu_{\max}$ were set to zero. This approximation is valid in several situations. Since the width of the Boltzmann distribution puts upper limits on the frequencies which enter significantly into a themally averaged decay, then if this limit is less than $\nu_{\max}$, the approximation is a good one. Also, the finite bandwidth of the excitation light source in a real experiment puts an upper limit on the frequencies which can be observed in a decay. Finally, an experiment may be limited in temporal resolution by factors other than the excitation pulse width. To the extent that these factors degrade the temporal resolution such that frequencies greater than $\nu_{\max}$ cannot be observed, the limit is valid.

Another approximation involving beat frequencies was made; we used a finite beat frequency resolution (ν_r) of 1.0, 0.1, 0.01, or 0.002 GHz, depending on the decay. This approximation is good on time scales much less than $\sim 1/\nu_r$.

Fourth, in calculating decays it clearly is necessary to divide the decays into discrete intervals of time. For the simulations we show here the increment of time used (t_r) was typically either 1.0 or 0.1 ps.

Finally, regarding the parameters appearing in Eq. (4.5), we took $\gamma = 0$. This was done to highlight the coherence effects relative to the lifetime decay. The rotational constants in the ground and excited electronic states were taken to be equal and the rotational energies given by[10]

$$E = BJ(J+1) + (A-B)K^2, \tag{4.10}$$

where A and B are appropriate rotational constants.

2. Polarization-dependent transients

Figure 4 shows, for $\hat{e}_1\|\hat{e}_2$ and $\hat{e}_1\perp\hat{e}_2$, calculated decays corresponding to a sample of prolate symmetric top molecules about the size of t-stilbene ($A = 2.678$ GHz, $B = 0.252$ GHz), at a temperature of 5 K. Each of the four pairs of decays corresponds to one of the four cases treated in Tables I and II. Also shown is an example of $I(\|) + 2I(\perp)$ for the $(\perp,\perp)$ case. Clearly, the transients are gone in this decay.

It is evident from Fig. 4 that the $(\|,\|)$ case, which has been considered in Ref. 1 and Sec. II, is not the only case for which polarization-dependent early-time transients and later-time recurrences occur as manifestations of the thermal averaging of rotational coherence. In fact, all four cases exhibit such behavior. As we have argued,[1] the behavior in the $(\|,\|)$ case can be readily understood in that (1) all beat frequencies entering into $I(t,\hat{e}_1,\hat{e}_2,T)$ are integer multiples of $2B$ (see Sec. II), and that (2) all the f's (see Table I) in Eq. (4.6) have the same sign when $\hat{e}_1\|\hat{e}_2$ or $\hat{e}_1\perp\hat{e}_2$. These two facts allow for constructive interference between all the beat components contributing to the thermally averaged decay at times $n/(2B)$, $n = 0,1,2,\ldots$. At times $m/(4B)$, $m = 1,3,5,\ldots$, all cosine terms with beat frequencies equal to $2BJ_0$ (see Sec. II) have signs opposite to the cosine terms with frequencies $2B(J_0+1)$ [because $\cos(mJ_0\pi) = -\cos[m(J_0+1)\pi]$, while having coefficients that are roughly equal in magnitude (see Table I). These terms, therefore, cancel each other out. The cosine terms with frequencies $2B(2J_0+1)$, however, always equal -1 at times $m/(4B)$, $m = 1,3,\ldots$. Hence, all these terms constructively interfere at such times and give rise to transients that are opposite in polarity and somewhat smaller in magnitude than the full recurrences that occur at times $n/(2B)$. At times very much different than $n/(2B)$ and $m/(4B)$, the summation of the many cosine terms in $I(t,\hat{e}_1,\hat{e}_2,T)$ tends toward zero, owing to destructive interference.

The explanation for the recurrence behavior in the $(\|,\|)$ case is just as valid for the $(\|,\perp)$ case. The same beat frequencies obtain in each case. And, the f coefficients in the $(\|,\perp)$ case are just $-1/2$ times the coefficients in the $(\|,\|)$ case (see Table I). Consequently, the same arguments for how the transients arise apply. The main difference in decays between the two cases, of course, is that, for a given orienta-

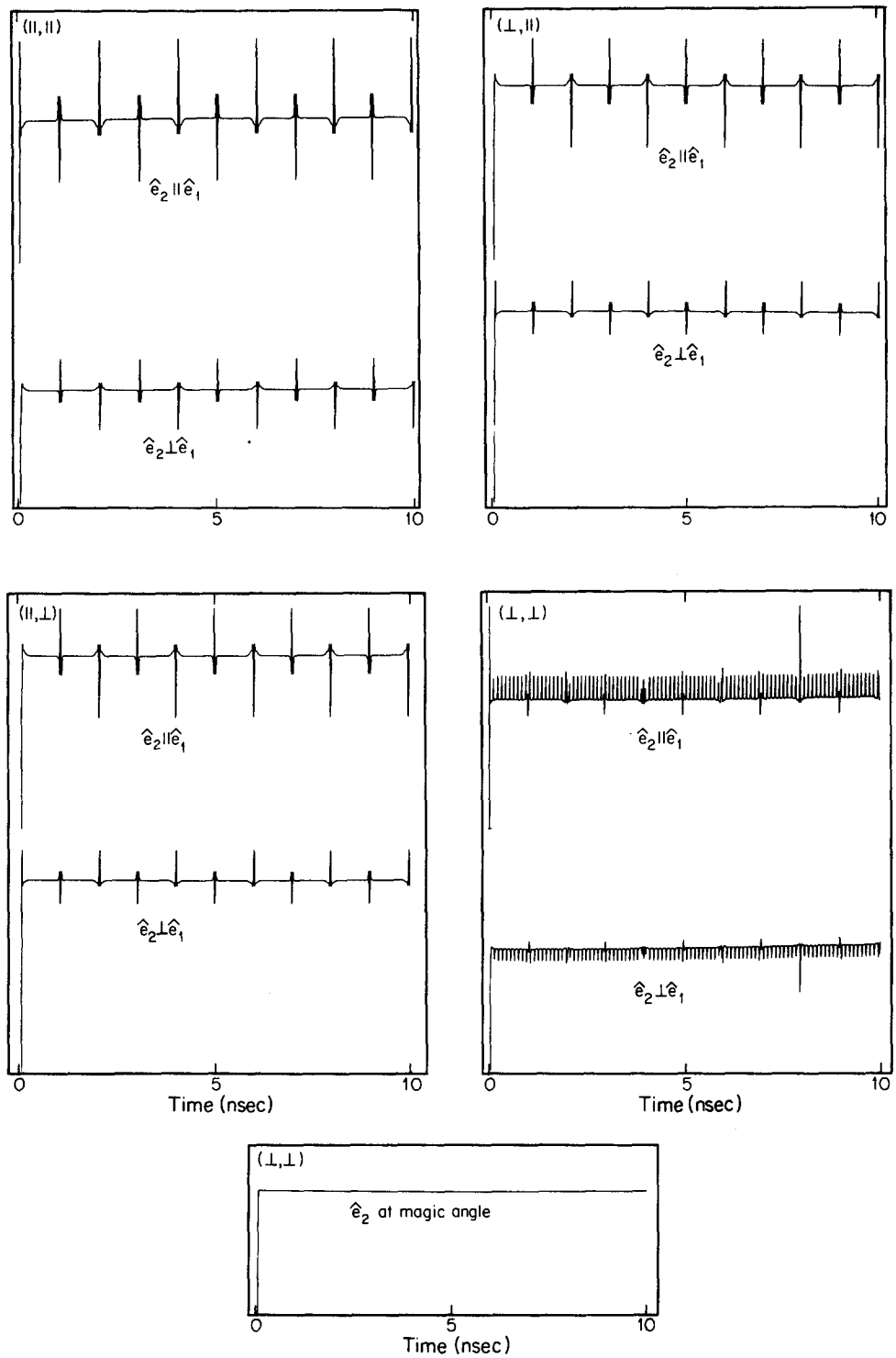

FIG. 4. Rotational coherence effects in the time-resolved fluorescence of thermal samples of symmetric top molecules. The decays shown represent the four absorption-emission dipole cases treated in Sec. IV B, with $\hat{e}_2||\hat{e}_1$ and $\hat{e}_2\perp\hat{e}_1$ for each. At the bottom of the figure is a calculated (⊥,⊥) decay for $\hat{e}_2$ at 54.7° to $\hat{e}_1$ (i.e., the magic angle) to show the absence of coherence effects for this orientation of the polarization. For all traces $\gamma = 0$ (to highlight the transients associated with the rotational coherence, we do not include the population decay of the excited states), $A = 2.678$ and $B = 0.252$ GHz, $T = 5$ K, $\nu_r = 0.002$ GHz, $\nu_{max} = 99.9$ GHz, $t_r = 0.1$ ps, and $J_0^{max} = 500$. The intensities of the two decays corresponding to a particular dipole case are true relative intensities. Similarly, the magic angle decay at the bottom has a true relative amplitude with respect to the other two (⊥,⊥) decays.

tion of $\hat{e}_1$ relative to $\hat{e}_2$, the polarities of the transients in the (||,⊥) case are opposite to those occurring at the same times in the (||,||) case. In addition, the magnitudes of transients relative to the "D.C." portion of the decay can be different for the two cases (see Fig. 4).

While the beat frequencies in the (⊥,||) case are the same as in the (||,||) and (||,⊥) cases, the f factors are different, more numerous, and more complicated in form (see Table II). Moreover, in the (⊥,||) case one cannot assert, as in the (||,||) and (||,⊥) cases, that all the f's have the same signs when $\hat{e}_1||\hat{e}_2$ or $\hat{e}_1\perp\hat{e}_2$. This implies that *complete* constructive interference between every cosine term in a thermally averaged (⊥,||) decay does not occur at any time. Despite this, however, Fig. 4 indicates that partial constructive interferences do occur, giving rise to recurrence behavior. (Note that even though the constructive interferences are partial, the recurrences are full.) That these recurrences occur at the same times as in the (||,||) and (||,⊥) cases is a result of the fact that the beat frequencies in all three cases are identical. A last point about the (⊥,||) case is that it appears to give rise to decays that are the same as the decays of the (||,⊥) case. This similarity is not exact, but it is very close. One can see

how it arises by comparing the f factors for the two cases (Tables I and II) in the limit of $J_0, K_0 \gg 1$, in which limit the two cases become identical.

The $(\perp,\perp)$ case, by Fig. 4, is clearly quite different from the other cases. The main reason for this is that for every value of J_0, K_0 in the $(\perp,\perp)$ case, there are ten different beat frequencies falling into three classes: (1) those which are integral multiples of $2B$; (2) the frequencies $4(A-B)K_0$, and (3) those frequencies which involve J_0, K_0, $2B$, and $4(A-B)$. This situation gives rise to four types of recurrences in the $(\perp,\perp)$ decays. Two types are analogous to the kinds that are present in the other three cases. These occur at times $n/(2B)$, $n = 0,1,2,...$, and $m/(4B)$, $m = 1,3,5,...$, respectively, and arise from the first class of beat frequencies listed above. The third type is associated with the second class of beat frequencies. These recurrences occur at times $n'/[4(A-B)]$, $n' = 1,2,...$. The fourth type of recurrence occurs at times when $n/(2B)$ and $n'/[4(A-B)]$ coincide (or nearly coincide). At such times all three types of beat frequencies contribute to a transient which is a full recurrence (or nearly a full recurrence) of the $t = 0$ intensity. One such recurrence can be seen in Fig. 4. Notably, the third class of beat frequency listed above in general only contributes to this fourth type of transient; because B and $(A-B)$ are not generally integer multiples of each other, beat frequencies in the third class are not commensurable with other frequencies in the same class.

3. Dependences of transients on rotational constants and temperature

In the preceding section we considered the general form of the decays that arise as a result of purely rotational coherence in samples of symmetric top molecules. In this section we undertake a more quantitative evaluation of the two most important quantities associated with such decays: (1) the time scales of the transients in the decays, and (2) the magnitudes of such transients relative to the D.C. intensities of the decays. Of particular interest is the dependence of these quantities on molecular geometry (i.e., rotational constants), on sample temperature, and on the direction of absorption and emission transition dipoles. Our aim here is not to be comprehensive in the assessment of such dependences, but to give the reader a general idea of the trends involved.

Figure 5 pertains to the effect of rotational constants and temperature on the time scale of the transients associated with rotational coherence. The simulations shown correspond to the fluorescence anisotropy, $r(t)$, near $t = 0$ for a symmetric top with $(\parallel,\parallel)$ transition dipoles. The upper portion of the figure shows the transients becoming narrower in time as the B rotational constant increases in magnitude. The lower portion shows a very similar effect on the transients as the sample temperature increases. Given in the figure caption are the temporal widths (Δt) at half-maximum of the transients. [Note that the widths of the transients at later time, i.e., the recurrences in the decays, are just twice the width of the corresponding $t = 0$ transient. This follows from Eqs. (4.6) and (4.7) and from the fact that $\cos\phi = \cos(-\phi) = \cos(n2\pi + \phi) = \cos(n2\pi - \phi)$, where n is an integer.] From these values for Δt it can be shown that in the upper part of the figure

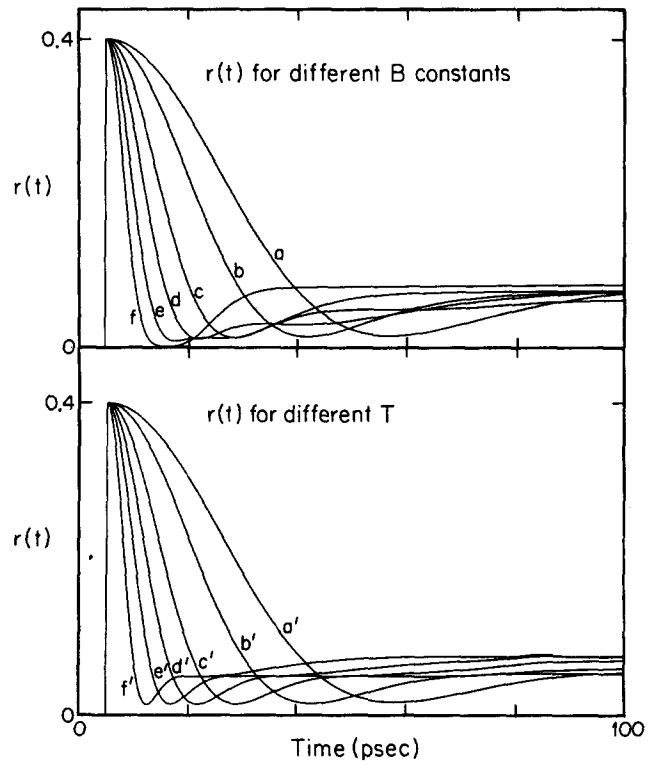

FIG. 5. (Top) Early time behavior of $r(t)$ as a function of the B rotational constant of a symmetric top molecule in the $(\parallel,\parallel)$ dipole case. For all traces $A = 2.678$, $T = 5$ K, $\nu_r = 0.002$ GHz, $\nu_{max} = 99.9$ GHz, $t_r = 0.1$ ps, and $J_0^{max} = 500$. For traces a through f, respectively, $B = 0.05$, 0.1, 0.252, 0.5, 1.0, and 2.0 GHz, and Δt (see the text) equals 23.4, 16.5, 10.5, 7.5, 5.4, and 3.9 ps. (Bottom) Early time behavior of $r(t)$ as a function of temperature for the $(\parallel,\parallel)$ case of a symmetric top molecule. For all traces A, ν_{max}, t_r, ν_r, and J_0^{max} are the same as above, and $B = 0.252$ GHz. For traces a' through f', respectively, $T = 1$, 2, 5, 10, 20, and 50 K, and $\Delta t = 23.3$, 16.5, 10.5, 7.5, 5.3, and 3.4 ps.

$$\Delta t \sim \frac{1}{\sqrt{B}} \tag{4.11a}$$

and in the lower

$$\Delta t \sim \frac{1}{\sqrt{T}}. \tag{4.11b}$$

Qualitatively, it is easy to understand such behavior in terms of the bandwidth of the beat frequencies contributing to the thermally averaged decays. Since the beat frequencies in the $(\parallel,\parallel)$ case are proportional to B, then as B increases, the beat frequency bandwidth increases. Similarly, since higher T favors higher J_0 values and since the beat frequencies in the $(\parallel,\parallel)$ case are proportional to J_0, then increasing T also increases the bandwidth. An increased bandwidth in the frequency domain results in narrower transients in the time domain. Thus, one can understand qualitatively the trends of Fig. 5. Quantitatively, it is instructive to derive (approximate) analytic expressions for the early time behavior of $r(t)$ in the $(\parallel,\parallel)$ case, expressions involving only t, T, and the rotational constants as variables. This is done in an appendix to this paper. The result (valid at early time) is a sum of the followng form:

$$r^{\|,\|}(t) = K + \sum_{i=1}^{N} g_i(A,B)\cos(4\pi t\sqrt{Bk_BTy_i}) + h_i(A,B)\cos(8\pi t\sqrt{Bk_BTy_i}), \quad (4.12)$$

where the y_i and K are constants, $g_i(A,B)$ and $h_i(A,B)$ are functions of A and B only, and where the greater N is, the better Eq. (4.12) approximates the actual decay. The full details pertaining to the expression may be found in the Appendix. The important point here is that the arguments of the cosine terms are all proportional to $t\sqrt{Bk_BT}$. Thus, Eq. (4.12) verifies the numerically deduced temperature dependence of the transients. Furthermore, although it predicts a somewhat complicated dependence of time scale on rotational constants, it does show that for the ($\|,\|$) case, the B constant has the greatest influence, and that the time scale goes approximately with $1/\sqrt{B}$.

Since the modulation terms in the ($\|,\perp$) case have the same frequencies as those in the ($\|,\|$) case and the corresponding f values differ only by a constant factor (see Table I), one expects the transients in the ($\|,\perp$) case to occur on the same time scale as those in the ($\|,\|$) case. The ($\perp,\|$) case, too, is characterized by the same beat frequencies as in the ($\|,\|$) and ($\|,\perp$) cases. One might expect its early time transients to occur on a nearly identical time scale. On the other hand, the more complicated ($\perp,\perp$) case with ten beat frequencies, some involving both rotational constants, would be expected to have significantly different transients. All these expectations are verified by numerical simulations. The simulations of Fig. 6, calculated by making use of the same rotational constants as used to generate Fig. 4, reveal that transients in the ($\|,\|$), ($\|,\perp$), and ($\perp,\|$) cases all decay at the same rate. At the same temperature, however, the ($\perp,\perp$) transient decays significantly faster. This has to do with the fact that some beat frequencies in the ($\perp,\perp$) case involve the larger rotational constant, A.

Table III pertains to the effect of rotational constants and temperature on the relative magnitude of rotational coherence transients. Two molecular geometries (very prolate and very oblate) and two temperatures (1 and 50 K) were considered for the four dipole cases. Since different types of transients occur within each case, the relative magnitudes of these different types are given. In all cases, the value given corresponds to the difference between the fluorescence intensity at transient peak and that of the flat part of the decay divided by the "flat" intensity:

$$I_{\text{rel}} = \frac{I_{\text{transient}} - I_{\text{flat}}}{I_{\text{flat}}}.$$

From the table one can see that in all dipole cases, and for the prolate and oblate tops, the relative magnitudes of transients do not change very much with temperature. More of an effect is evident in going from the prolate geometry to the oblate one; the relative intensities in the prolate case are larger than in the oblate one. One can understand this behavior by noting that for a prolate top there is a bias in the Boltzmann factor toward low values of K_0, while for an oblate rotor the bias is towards $K_0 \simeq J_0$. Now, from Tables I and II *all* but one of the f factors for nonzero beat frequencies approach zero as K_0 approaches J_0. In contrast, some of the f factors are at their maximum for $K_0 = 0$. Thus, there is a bias towards greater beat modulation (and, hence, greater relative magnitudes of transients) in the decays of prolate tops relative to oblate ones.

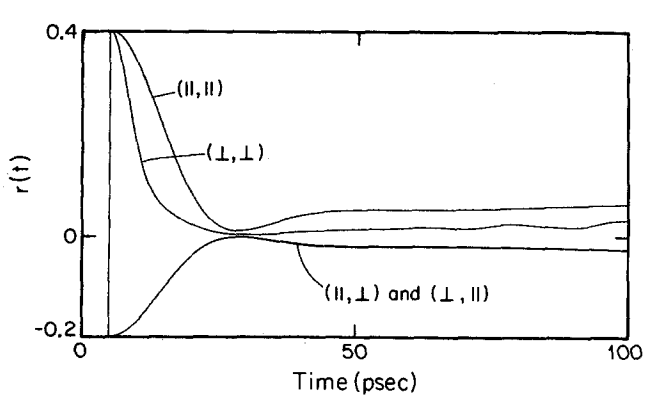

FIG. 6. Early time $r(t)$ for the four symmetric top dipole cases treated in the text. Each trace was calculated with $A = 2.678$ GHz, $B = 0.252$ GHz, $T = 5$ K, $\nu_r = 1$ GHz, $\nu_{\max} = 499.9$ GHz, and $t_r = 0.1$ ps. Δt for the ($\|,\|$), ($\|,\perp$), and ($\perp,\|$) early time anisotropy is 10.5 ps. For the ($\perp,\perp$) case Δt is 4.7 ps.

V. ROTATIONAL COHERENCE EFFECTS IN ASYMMETRIC TOP MOLECULES

In this section we treat the same coherence phenomenon that was dealt with in Sec. IV, except that now we consider asymmetric top molecules. The changes to be made from the treatment of the previous section occur in the form of the rotational eigenfunctions. These eigenfunctions are linear combinations of symmetric top eigenfunctions[35]:

$$|J\tau M\rangle = \sum_{K=-J}^{J} a(J\tau K)|JKM\rangle, \quad (5.1)$$

where τ, an index distinguishing between rotational levels of the same J but different energy, runs from $-J$ to J, and where the $a(J\tau K)$ are real, orthonormal coefficients,

$$\sum_{\tau} a(J\tau K)a(J\tau K') = \delta_{KK'}, \quad (5.2)$$

$$\sum_{K} a(J\tau K)a(J\tau' K) = \delta_{\tau\tau'}, \quad (5.3)$$

obtained by diagonalizing the asymmetric top rotational Hamiltonian matrix expressed in the symmetric top basis.

As in Sec. IV, we eventually shall have to use Eq. (3.20) to find $I(t,\hat{e}_1,\hat{e}_2,T)$. The summations Σ_{Γ_i} appearing in Eq. (3.20) are equivalent now to $\Sigma_{J_i\tau_i}$.

The analog to the symmetric top Eq. (4.1) can be obtained for the asymmetric top by substituting states of the form $|\Gamma_i\, M_i\rangle = |S_i v_i; J_i \tau_i\, M_i\rangle$ in Eq. (3.15) and making use of Eq. (5.1). One finds that one can express the asymmetric top $A(Q_i)$ coefficients as linear combinations of symmetric top $A(Q_i)$ coefficients:

TABLE III. Relative intensities of transients associated with rotational coherence in prolate and oblate symmetric top molecules at $T = 1$ and $T = 50$ K.[a]

		($\parallel$,$\parallel$) dipole case $n/(2B)$ transients[b]		$m/(4B)$ transients[c]	
		prolate[d]	oblate[e]	prolate	oblate
$T = 1$ K	$\hat{e}_2\parallel\hat{e}_1$	0.557	0.384	−0.423	−0.121
	$\hat{e}_2\perp\hat{e}_2$	−0.349	−0.294	0.266	0.093
$T = 50$ K	$\hat{e}_2\parallel\hat{e}_1$	0.567	0.378	−0.439	−0.131
	$\hat{e}_2\perp\hat{e}_2$	−0.352	−0.291	0.272	0.101
		($\parallel$,$\perp$) dipole case $n/(2B)$ transients		$m/(4B)$ transients	
		prolate	oblate	prolate	oblate
$T = 1$ K	$\hat{e}_2\parallel\hat{e}_1$	−0.349	−0.294	0.266	0.093
	$\hat{e}_2\perp\hat{e}_1$	0.154	0.116	−0.118	−0.037
$T = 50$ K	$\hat{e}_2\parallel\hat{e}_1$	−0.352	−0.291	0.272	0.101
	$\hat{e}_2\perp\hat{e}_1$	0.157	0.115	0.121	−0.040
		($\perp$,$\parallel$) dipole case $n/(2B)$ transients		$m/(4B)$ transients	
		prolate	oblate	prolate	oblate
$T = 1$ K	$\hat{e}_2\parallel\hat{e}_1$	−0.355	−0.289	0.255	0.100
	$\hat{e}_2\perp\hat{e}_1$	0.159	0.113	−0.115	−0.039
$T = 50$ K	$\hat{e}_2\parallel\hat{e}_1$	−0.352	−0.291	0.272	0.101
	$\hat{e}_2\perp\hat{e}_1$	0.157	0.115	0.121	−0.040

		$t = 0$ transient		($\perp$,$\perp$) dipole case $n/(2B)$ transients		$m/(4B)$ transients		$n/[4(A-B)]$ transients[f]	
		prolate	oblate	prolate	oblate	prolate	oblate	prolate	oblate
$T = 1$ K	$\hat{e}_2\parallel\hat{e}_1$	(0.736)[g]	(0.659)	(0.537)[h]	(0.106)	(−0.133)	(−0.044)	(0.187)	(0.060)
	$\hat{e}_2\perp\hat{e}_1$	(−0.388)	(−0.373)	(−0.283)[h]	(−0.060)	(0.060)	(0.025)	(−0.098)	(0.033)
$T = 50$ K	$\hat{e}_2\parallel\hat{e}_1$	0.735	0.672	0.158	0.114	−0.121	−0.040	0.180	0.060
	$\hat{e}_2\perp\hat{e}_1$	−0.388	−0.376	−0.083	−0.064	0.065	0.022	−0.094	−0.033

[a] The $I_{\rm rel}$ values defined in Sec. IV C 3 of the text.
[b] $n = 1,2,3,\ldots$.
[c] $m = 1,3,5,\ldots$.
[d] The constants of the prolate molecule were 2.678, 0.252, and 0.252 GHz for A, B, and C, respectively.
[e] The constants of the oblate molecule were 1.0, 1.0, and 0.17 GHz for A, B, and C, respectively.
[f] $n = 1,2,3,\ldots$, and in the oblate case replace $(A–B)$ with $(B–C)$.
[g] Parentheses around a value indicate that it is somewhat approximate in that there may be contributions from more than one type of transient reflected in the value.
[h] These values are very uncertain owing to an extreme of the situation mentioned in footnote g.

$$ {}^{\Gamma_i\Gamma_i'}_{L_iL_i'}A\,{}^{\Gamma_k\Gamma_k'}_{L_kL_k'}(Q_i) = \delta_{l_il_k}\sum_{K_iK_i'}\sum_{K_kK_k'} {}^{\gamma_i\gamma_i'}_{L_iL_i'}A\,{}^{\gamma_k\gamma_k'}_{L_kL_k'}(Q_i) \times a(J_i\tau_i K_i)a(J_i'\tau_i'K_i')a(J_k\tau_k K_k)a(J_k'\tau_k'K_k'), \tag{5.4} $$

where we have used the γ's to denote symmetric top quantum numbers

$$ |\gamma_i\, M_i\rangle \equiv |S_i v_i; J_i\, K_i\, M_i\rangle, $$

and where the $A(Q_i)$ coefficients on the right-hand side are given by Eq. (4.1). Hence, in evaluating Eq. (3.20) using Eq. (5.4), we can use some of the results previously obtained in Sec. IV for the symmetric top. After some straightforward algebra the general expression for an asymmetric top can be shown to be

$$ I(t,\hat{e}_1,\hat{e}_2,T) = \sum_{\Gamma_0}\frac{G(\Gamma_0)e^{-E_{\Gamma_0}/k_BT}}{Q}\Bigg[\sum_{\Gamma_1\Gamma_1'}\sum_{q_1q_1'}\sum_{q_2q_2'}\sum_{L_1}\sum_{K_1K_1'}\sum_{K_1''K_1'''}\sum_{K_0K_0'} D_{00}^{(L_1)}(\phi,\theta,0) $$
$$ \times(-1)^{J_0+J_1+J_1'+K_1+K_1''+K_0'+Q_2+Q_1}(2J_0+1)(2J_1+1)(2J_1'+1)(2L_1+1) $$
$$ \times a(J_0\tau_0K_0)a(J_0\tau_0K_0')a(J_1\tau_1K_1)a(J_1'\tau_1'K_1')a(J_1\tau_1K_1'')a(J_1'\tau_1'K_1''') $$
$$ \times\mu_1^{1,q_1}\mu_1^{1,-q_1'}\mu_2^{1,q_2}\mu_2^{1,-q_2'}\begin{pmatrix}1 & 1 & L_1\\ Q_1 & -Q_1 & 0\end{pmatrix}\begin{pmatrix}1 & 1 & L_1\\ Q_2 & -Q_2 & 0\end{pmatrix} $$

$$\times\begin{pmatrix} L_1 & 1 & 1 \\ q_2'-q_2 & -q_2' & q_2 \end{pmatrix}\begin{pmatrix} J_1 & 1 & J_0 \\ -K_1 & q_1 & K_0 \end{pmatrix}\begin{pmatrix} J_0 & 1 & J_1' \\ -K_0' & -q_1' & K_1' \end{pmatrix}$$

$$\times\begin{pmatrix} J_1 & J_1' & L_1 \\ K_1'' & K_1''' & q_2-q_2' \end{pmatrix}\begin{Bmatrix} J_1 & J_1' & L_1 \\ 1 & 1 & J_0 \end{Bmatrix}\Bigg] e^{-i\omega_{\Gamma_1\Gamma_1'}t}e^{-\gamma t}. \tag{5.5}$$

A. General results

As from the symmetric top Eq. (4.5), a number of results can be obtained from the general expression (5.5). Again, there are the well known selection rules for J. And, the 3-j symbols give $K_1 = K_0 + q_1$, $K_1' = K_0' + q_1'$, $K_1''' = K_1'' + q_2 - q_2'$, and $L_1 = 0$, 1, or 2 ($L_1 = 0$ or 2 if linear polarizations are involved).

The analog to Eqs. (4.6) and (4.7) is true for the asymmetric top. That is, given

$$I(t,\hat{e}_1,\hat{e}_2,T) = C\sum_{\Gamma_0}\frac{G(\Gamma_0)e^{-E_{\Gamma_0}/k_BT}}{Q} \times\sum_{\Gamma_1,\Gamma_1'} e^{-i\omega_{\Gamma_1\Gamma_1'}t}e^{-\gamma t}f(J_0,J_1,J_1',\tau_0,\tau_1,\tau_1') \tag{5.6}$$

then one can prove that the f's are real and that

$$f(J_0,J_1,J_1',\tau_0,\tau_1,\tau_1') = f(J_0,J_1',J_1,\tau_0,\tau_1',\tau_1), \tag{5.7}$$

if μ_1 and μ_2 are along principal axes of the molecule.

Third, if $L_1 = 0$, then $J_1 = J_1'$ and $K_1'' = K_1'''$. The latter equality, in turn, gives the following expression for the sums over K_1'' and K_1''':

$$\sum_{K_1'',K_1'''}(-1)^{K_1''}a(J_1\tau_1K_1'')a(J_1\tau_1'K_1''') \times\begin{pmatrix} J_1 & J_1 & 0 \\ K_1''' & -K_1'' & 0 \end{pmatrix}\delta_{K_1'',K_1'''} = \frac{(-1)^{J_1}}{\sqrt{2J_1+1}}\delta_{\tau_1',\tau_1}, \tag{5.8}$$

where we have evaluated the 3-j symbol and used the orthonormality of the a's. Since $J_1 = J_1'$ and $\tau_1 = \tau_1'$ for all $L_1 = 0$ terms, all modulation terms in Eq. (5.5) correspond to $L_1 = 1$ or 2.

The form of Eq. (4.5) makes it clear that the analog to symmetric top expression (4.8) is true for the asymmetric top. That is, for linear polarizations and $\omega_{\Gamma_1\Gamma_1'} \neq 0$,

$$f_\perp(J_0,J_1,J_1',\tau_0,\tau_1,\tau_1') = -\tfrac{1}{2}f_\parallel(J_0,J_1,J_1',\tau_0,\tau_1,\tau_1'). \tag{5.9}$$

Therefore, again, beat modulations have opposite phases for parallel vs perpendicular detection polarization. And, $I(\parallel) + 2I(\perp)$—total fluorescence or fluorescence collected through a magic angle polarizer—is unmodulated in time.

Values for $r(0)$, the fluorescence anisotropy at $t = 0$ can be derived for the asymmetric top from Eq. (5.5). The results are the same as those for the symmetric top; with the absorption and emission dipoles along principal rotation axes of the molecule, then if the dipoles are parallel to each other, $r(0) = 0.4$, while if they are perpendicular, $r(0) = -0.2$.

B. Numerical simulations

The major observable manifestations of rotational coherence in asymmetric top molecules are not wholly different than those associated with symmetric top molecules. In some cases, however, one might envision one significant difference. Specifically, in going from a symmetric top to an asymmetric top with the same average rotational constants, same transition dipole directions, and at the same temperature a decrease in the magnitude of the later time transients should occur. This effect should arise because the rotational energy spacings in an asymmetric top are less regular than in a symmetric top molecule. It is our aim in this section to examine this effect via numerical simulation of decays. The rotational constants used in the simulations are for illustration only, and more quantitative comparison with experiments will be made in paper II.

1. Approximations

Numerical evaluation of Eq. (5.5) is considerably more time consuming than evaluation of the symmetric top expression Eq. (4.5). This is true even for molecules of high symmetry. As a consequence of the increased computation time, we have chosen $J_0^{\max}$ to be $\leqslant 50$, considerably smaller values than that used in the symmetric top calculations. Accordingly, we only present calculated decays for relatively low sample temperatures. We have checked these decays for possible J_0-truncation artifacts by examining symmetric top decays, generated using the same temperature and the same average rotational constants, as a function of $J_0^{\max}$. Artifacts were found to be insignificant.

The other types of approximations enumerated in Sec. IV C 1 and pertaining to ν_r, $\nu_{\max}$, t_r, and γ for the symmetric top simulations were also used in the calculations of decays for asymmetric tops.

2. Results

Shown in Fig. 7 are $r(t)$ traces for the (A,A) dipole case of near-prolate asymmetric top molecules that show the damping of recurrences that occurs as molecules become more asymmetric. Parameters used in the calculation of these traces are given in the figure caption. From the figure it is clear that the degree of asymmetry of a molecule has a significant effect in reducing the magnitude of the transients. Nevertheless, the transients are still present. Moreover, one sees that the times at which the recurrences occur change very little as the degree of asymmetry changes. This is so because in the simulations we have kept the sum of $B + C$ constant. Using approximate relations for the rotational energy of asymmetric tops,[10] one expects the recurrences in the (A,A) dipole case of near-prolate tops to be spaced by $1/(B + C)$.

VI. ROTATIONAL COHERENCE AS TIME-DEPENDENT MOLECULAR ORIENTATION

The concern in this section is to demonstrate the fact that rotational coherence effects reflect the temporal evolution of the spatial orientation of excited molecules in a gaseous sample. Consider $\rho(\Omega,t)$, the excited state orientation probability density as a function of time for a sample of symmetric top molecules prepared by coherent excitation with principally polarized light. $\rho(\Omega,t)$ can be obtained from σ_1 by using the following relation:

$$\rho(\Omega,t) = \mathrm{Tr}\{\sigma_1 \not{\rho}\}, \tag{6.1}$$

where

$$\not{\rho} \equiv \begin{pmatrix} |\Psi_{000}(\Omega)|^2 & \cdots & \Psi_{000}(\Omega)^*\Psi_{J_1K_1M_1}(\Omega) & \cdots \\ \vdots & \ddots & \vdots & \vdots \\ \Psi_{000}(\Omega)\Psi^*_{J_1K_1M_1}(\Omega) & \cdots & |\Psi_{J_1K_1M_1}(\Omega)|^2 & \cdots \\ \vdots & \vdots & \vdots & \vdots \end{pmatrix} \tag{6.2}$$

and the $\Psi_{J_1K_1M_1}(\Omega)$ are symmetric top eigenfunctions. Ω denotes the Euler angles (α,β,γ) that give the orientation of the molecule-fixed axis system with respect to the laboratory-fixed system.[30] [We use α,β,γ rather than ϕ,θ,χ since the latter are used in conjunction with the direction of the axis of $\hat{e}_1$. See Eq. (3.21).] Using Eq. (6.1) along with Eqs. (3.9), (3.13), and (3.17), expressing the symmetric top eigenfunctions in terms of elements of the Wigner rotation matrices,[30] and using Eq. (4.3.2) of Ref. 30, one obtains

$$\rho(\Omega,t) = \frac{1}{8\pi^2}\sum \frac{G(\Gamma_0)e^{-E_{\Gamma_0}/k_BT}}{Q}(-1)^{J_1+K_1'} \times [(2J_0+1)(2J_1+1)(2J_1'+1)]^{1/2} \times \begin{pmatrix} J_1 & J_1' & L_1 \\ K_1 & -K_1' & l \end{pmatrix} \left[{}^{\Gamma_1\Gamma_1'}_{L,0} A^{\Gamma_0\Gamma_0}_{00}(Q_1)\right] \times (e^{-i\omega_{\Gamma_1\Gamma_1'}t}e^{-\gamma t}) D^{(L_1)}_{0-l}(\Omega), \tag{6.3}$$

with the $A(Q_1)$ coefficients given by Eq. (4.3), and where the summation is over all indices. From a comparison of Eqs. (6.3) and (4.5), it is clear that the orientation of excited molecules in the sample evolves in a manner similar to the directional fluorescence emanating from the sample; $\rho(\Omega,t)$ is temporally modulated by terms of identical frequency (the $\omega_{\Gamma_1\Gamma_1'}$) to those modulating $I(t,\hat{e}_1,\hat{e}_2,T)$ of Eq. (4.5). *This suggests that the transients associated with rotational coherence are manifestations of the temporal evolution of the angular orientation of molecules.*

To demonstrate this point more explicitly consider a specific case of Eq. (6.3) corresponding to the linearly polarized (Z axis) excitation of a parallel-type transition. In this case, at $t=0$, $\rho(\Omega,t)\sim\cos^2(\beta)$. [This result is obtained by using (4.3) and $t=0$ in Eq. (6.3).] As time goes on the probability density changes its shape according to

$$\rho(\Omega,t) = e^{-\gamma t}\sum_{\Gamma_0}\frac{G(\Gamma_0)e^{-E_{\Gamma_0}/k_BT}}{Q} \times [A_1(\Gamma_0) + A_2(\Gamma_0)(3\cos^2\beta - 1) + B(\Gamma_0,t)(3\cos^2\beta - 1)], \tag{6.4}$$

where $A_1(\Gamma_0)$ and $A_2(\Gamma_0)$ are constant in time and space,

$$B(\Gamma_0,t) = \sum_{\Gamma_1,\Gamma_1',(\Gamma_1\neq\Gamma_1')} f(J_0,J_1,J_1',K_0)e^{-i\omega_{\Gamma_1\Gamma_1'}t}, \tag{6.5}$$

and the f's in Eq. (6.5) are the same (apart from a constant multiplication factor) as those in Table I that correspond to nonzero beat frequencies. Thus one sees the direct relationship between beats in fluorescence and molecular orientation. Not just the beat frequencies, but also the relative intensities of the modulation components contributing to a rotational coherence decay, are the same as those of the modulations in molecular orientation that occur upon pulsed excitation of a gaseous sample of molecules.

It is pertinent to note that $\rho(\Omega,t)$ has no dependence on the fluorescence process. It only depends on the details of the excitation. Thus, for example, although $\rho(\Omega,t)$ of Eq. (6.4) applies to both the $(\|,\|)$ and $(\|,\perp)$ cases of Sec. IV B, fluorescence decays in the two cases are different. Similarly, decays for $\hat{e}_1\|\hat{e}_2$ are different than those for $\hat{e}_1\perp\hat{e}_2$, even though the same $\rho(\Omega,t)$ characterizes each case. The point is that the actual form of a fluorescence decay arising in a situation of rotational coherence depends on the way in which one *probes* the time-dependent orientation of molecules in the sample.

Finally, it is noteworthy that rotational coherence, in as much as it reflects changing molecular orientation, is similar to other cases of quantum coherence.[3,11–19] A first example is quantum interference between Zeeman levels in isolated species. This situation is also characterized by excited species that undergo time-dependent reorientation, the manifestations of this reorientation being detection polarization-dependent quantum beats. The major difference between the two situations is that there is no time-dependent reorientation in the Zeeman case in the absence of an applied field. The cases of coherently prepared fine, or hyperfine levels are other situations wherein a time-dependent reorientation of species in the sample gives rise to polarization-dependent quantum beats. (That which evolves are the directions of electronic angular momentum vectors.) Moreover, as in the case of rotational coherence, the temporal evolution of the reorientation occurs in the absence of an applied field.

VII. A CLASSICAL TREATMENT OF ROTATIONAL COHERENCE

One's intuitive grasp of the physical situation manifested in purely rotational coherence can be strengthened by approaching the problem from a classical perspective. In doing so, one might also hope to be led to appropriate classical limits of the quantum mechanical results. In this section, we

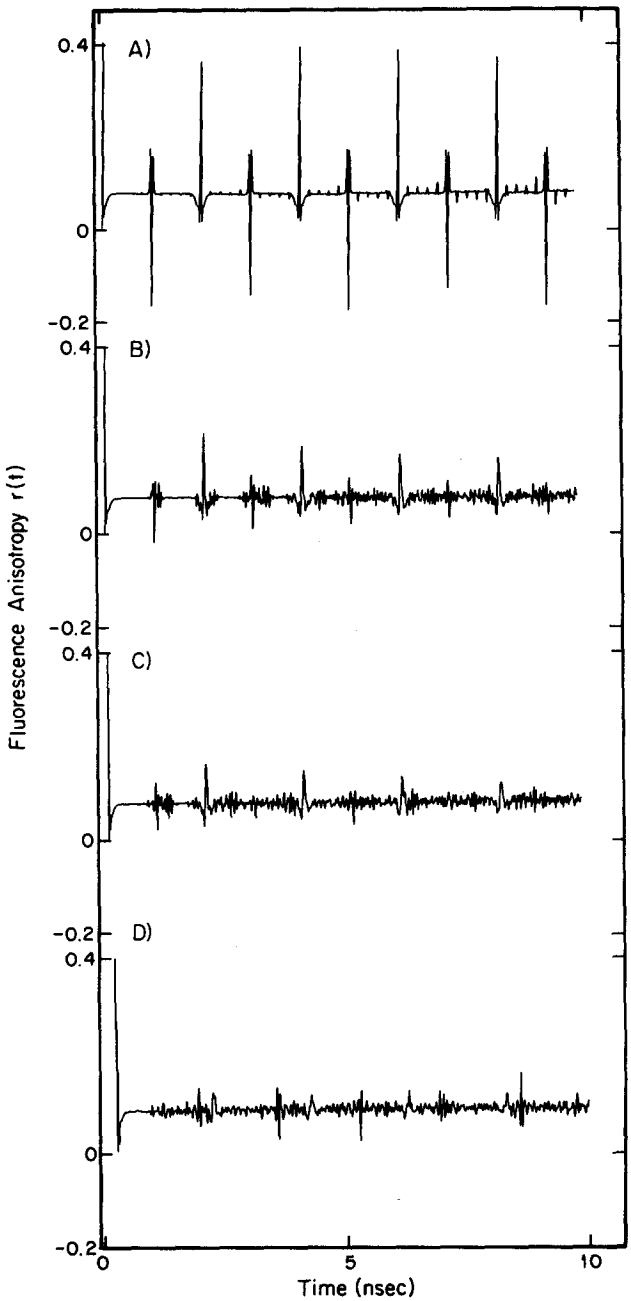

FIG. 7. The effect of molecular asymmetry on the recurrences associated with rotational coherence. All traces correspond to $r(t)$ for the (A,A) dipole case. For each trace $T = 5$ K, $\nu_r = 0.01$ GHz, $\nu_{max} = 49.9$ GHz, $t_r = 10$ ps, $A = 2.678$ GHz, and $B + C = 0.504$ GHz. For (A) through (D), respectively, $B = 0.252$ and $C = 0.252$, $B = 0.275$ and $C = 0.229$, $B = 0.300$ and $C = 0.204$, and $B = 0.350$ and $C = 0.154$ GHz. One notes that spurious transients of weak intensity appear in the symmetric top trace of Fig. 7(A). These arise as a result of ν_r being too large. Also, the large value of t_r used gives rise to small artifacts in the symmetric top trace (unequal intensities for equivalent transients). We show the particular symmetric top trace that we do because all the parameters used to calculate it (except B and C) are identical to those used to calculate the other three traces.

consider time-resolved fluorescence from classically rotating molecules. We show that there are significant correspondences between classical and quantal results, and that semiclassical expressions, derived by quantization of the classical results, provide a reasonably quantitative approximation of rotational coherence effects.

For classically rotating molecules having absorption and emission dipole moments denoted by $\mathbf{d}_1$ and $\mathbf{d}_2(t)$, respectively ($\mathbf{d}_1$ and $\mathbf{d}_2$, being vectors in the laboratory frame) the ensemble-averaged fluorescence signal as a function of time upon delta-function excitation is given by

$$I(t,\hat{e}_1,\hat{e}_2,T) \sim \langle(\hat{e}_1\cdot\mathbf{d}_1)^2[\hat{e}_2\cdot\mathbf{d}_2(t)]^2\rangle, \tag{7.1}$$

where $\hat{e}_1$ and $\hat{e}_2$ are the excitation and detection polarization, and the brackets denote the ensemble average at $t = 0$. Note that $\mathbf{d}_1$ does not depend on time because the only time at which is is pertinent is $t = 0$. [Equation (7.1) can be derived as the classical limit of Eq. (3.19) by using the method of Gordon[36] who has related line shape functions to molecular motion in the classical limit.] To evaluate Eq. (7.1) it is necessary to average over six variables in phase space corresponding to three orientational coordinates and three momentum coordinates. It shall be convenient to use the coordinates defined as follows:

(1) $L \equiv |\mathbf{L}|$, the magnitude of the angular momentum.

(2) L_z, the projection of $\mathbf{L}$ projected on the symmetry axis of the molecule.

(3) ϕ, the angle between the projection of $\mathbf{L}$ in the plane perpendicular to the molecular symmetry axis and the molecular x axis.

(4)–(6) α,β, and γ (defined as a group as Ω), the Euler angles[30] describing the orientation of a laboratory axis system rotated with respect to the molecule-fixed system. Using these coordinates one can completely specify the orientation of a molecule and its angular momentum.

To proceed we first perform the ensemble average over Ω, which average accounts for the isotropy of the sample. Following Ref. 37:

$$\langle[\hat{e}_1(\Omega)\cdot\mathbf{d}_1]^2[\hat{e}_2(\Omega)\cdot\mathbf{d}_2(t)]^2\rangle_\Omega = \sum_{ijkl}\langle e_{1,i}e_{1,j}\,e_{2,k}e_{2,l}\rangle_\Omega d_{1,i}d_{1,j}\,d_{2,k}(t)d_{2,l}(t), \tag{7.2}$$

where the $e_{1,i}$ and $e_{2,i}$ are Cartesian components of $\hat{e}_1$ and $\hat{e}_2$, respectively, and the $d_{1,i}$ and $d_{2,i}$ are analogous components of $\mathbf{d}_1$ and $\mathbf{d}_2$. We consider the two cases of linear polarizations corresponding to $\hat{e}_2\|\hat{e}_1$ and $\hat{e}_2\perp\hat{e}_1$. For $\hat{e}_2\|\hat{e}_1$, one has[37]

$$\langle e_{1,i}e_{1,j}\,e_{2,k}e_{2,l}\rangle_\Omega = \tfrac{1}{15}\{\delta_{ij}\,\delta_{kl} + \delta_{ik}\delta_{jl} + \delta_{il}\delta_{jk}\} \tag{7.3}$$

and for $\hat{e}_2\perp\hat{e}_1$,

$$\langle e_{1,i}e_{1,j}\,e_{2,k}e_{2,l}\rangle_\Omega = \tfrac{1}{30}\{4\delta_{ij}\,\delta_{kl} - \delta_{ik}\delta_{jl} - \delta_{il}\delta_{jk}\}. \tag{7.4}$$

Equation (7.2) becomes in the $\hat{e}_1\|\hat{e}_2$ case

$$\langle(\hat{e}_1\cdot\mathbf{d}_1)^2[\hat{e}_2\cdot\mathbf{d}_2(t)]^2\rangle_\Omega = \tfrac{1}{15}\{|\mathbf{d}_1|^2|\mathbf{d}_2|^2 + 2[\mathbf{d}_1\cdot\mathbf{d}_2(t)]^2\} \tag{7.5}$$

and in the $\hat{e}_1\perp\hat{e}_2$ case

$$\langle(\hat{e}_1\cdot\mathbf{d}_1)^2[\hat{e}_2\cdot\mathbf{d}_2(t)]^2\rangle_\Omega = \tfrac{1}{15}\{2|\mathbf{d}_1|^2|\mathbf{d}_2|^2 - [\mathbf{d}_1\cdot\mathbf{d}_2(t)]^2\}. \tag{7.6}$$

Equations (7.5) and (7.6) display two noteworthy characteristics. First, they show that the temporal evolution of the polarized fluorescence is determined by the correlation function $\{\mathbf{d}_1\cdot\mathbf{d}_2(t)\}^2$ ($|\mathbf{d}_1|^2|\mathbf{d}_2|^2$ is constant in time). But, this correlation function depends solely on the rotational dynamics of the molecule. The classical results, therefore, strengthen one's grasp of the connection between rotational motion and

polarization-dependent transients in fluorescence. Second, Eqs. (7.5) and (7.6), taken together, show that $I(\|) + 2I(\perp)$ has no temporal evolution attributable to rotational motion. This result is exactly the same as the quantum mechanical result.

To proceed further with the analysis, it is useful now to make specific assumptions about the molecule and its transition dipole moments. We shall consider the simplest case, corresponding to a symmetric top molecule (the classical rotational dynamics of which is well known[38]) with transition dipoles that are parallel to the molecule's symmetry axis [the $(\|,\|)$ case of Sec IV B and Table I]. It is straightforward in this case to show that

$$\mathbf{d}_1 \cdot \mathbf{d}_2(t) = |\mathbf{d}_1||\mathbf{d}_2| \left\{ \frac{L^2 - L_z^2}{L^2} \cos(Lt/I_x) + \frac{L_z^2}{L^2} \right\}, \tag{7.7}$$

where I_x is the principal moment of inertia of the molecule about an axis perpendicular to the symmetry axis.

One can now average Eqs. (7.5) and (7.6) over ϕ, L_z, and L. We assume Maxwell–Boltzmann statistics to obtain the probability density

$$\rho(\phi, L_z, L) = 2L\, e^{-(L^2/2I_x + L_z^2/2I')/k_B T}. \tag{7.8}$$

Equation (7.1), with Eqs. (7.7) and (7.8), and Eq. (7.5) or (7.6), gives

$$I^{\|,\|}(t, \hat{e}_1 \| \hat{e}_2) \sim \frac{2}{15} \int_0^\infty \int_{-L}^{L} \int_0^{2\pi} dL\, dL_z\, d\phi\, e^{-(L^2/2I_x + L_z^2/2I')/k_B T} \frac{1}{L^3}$$
$$\times \left\{ (L^4 + 2L_z^4 + (L^2 - L_z^2)^2) + 4L_z^2 (L^2 - L_z^2) \cos\left(\frac{L}{I_x} t\right) + (L^2 - L_z^2)^2 \cos\left(\frac{2L}{I_x} t\right) \right\}, \tag{7.9}$$

$$I^{\|,\|}(t, \hat{e}_1 \perp \hat{e}_2) \sim \frac{2}{15} \int_0^\infty \int_{-L}^{L} \int_0^{2\pi} dL\, dL_z\, d\phi\, e^{-(L^2/2I_x + L_z^2/2I')/k_B T} \frac{1}{L^3}$$
$$\times \left\{ (2L^4 - L_z^4 - \frac{(L^2 - L_z^2)^2}{2} - 2L_z^2 (L^2 - L_z^2) \cos\left(\frac{L}{I_x} t\right) - \frac{(L^2 - L_z^2)^2}{2} \cos\left(\frac{2L}{I_x} t\right) \right\}, \tag{7.10}$$

where $1/I' \equiv 1/I_z - 1/I_x$.

Equations (7.9) and (7.10) can be compared directly with the quantum expression, Eq. (4.6), by substituting appropriate f values from Table I into Eq. (4.6) and by using $L^2 = J_0(J_0+1)\hbar^2$, $L_z = K_0\hbar$, and $L/I_x = 2B\sqrt{J_0(J_0+1)}2\pi$. Upon doing so, one point of immediate note is that *the classical intensities have modulation terms in them*. Furthermore, the frequencies of these modulations have corresponding *quantum* beat frequencies [Eq. (4.6)]. To see this, note that for a given vaue of L in Eq. (7.9) or (7.10), there are two modulation terms in the fluorescence, having frequencies $2B\sqrt{J_0(J_0+1)}$ and $4B\sqrt{J_0(J_0+1)}$, respectively. There are three corresponding quantum beat frequencies $2BJ_0$, $2B(J_0+1)$, and $2B(2J_0+1)$. However, the two smaller beat frequencies approach the smaller classical frequency, in a relative sense, as $J_0 \to \infty$:

$$\lim_{J_0 \to \infty} \frac{2BJ_0}{2B\sqrt{J_0(J_0+1)}} = \frac{2B(J_0+1)}{2B\sqrt{J_0(J_0+1)}} = 1. \tag{7.11}$$

Similarly, the largest classical and quantal frequencies also approach each other:

$$\lim_{J_0 \to \infty} \frac{2B(2J_0+1)}{4B\sqrt{J_0(J_0+1)}} = 1. \tag{7.12}$$

Thus, there is a correspondence between modulation frequencies in the classical and quantal cases. It turns out, moreover, that this correspondence between modulations extends to their Fourier amplitudes, as well. That is, as $J_0 \to \infty$, the amplitude of the classical term $\cos[2B\sqrt{J_0(J_0+1)}2\pi t]$ is equal to the sum of the amplitudes of the quantum beat terms $\cos(2BJ_0 2\pi t)$ and $\cos[2B(J_0+1)2\pi t]$, and the amplitude of the $\cos[4B\sqrt{J_0(J_0+1)}2\pi t]$ classical modulation is equal to that of the quantal term $\cos[2B(2J_0+1)2\pi t]$. Therefore, if one is allowed to make the correspondences we have made between classical and quantal frequencies, *then the quantal Eq. (4.6) goes over to Eq. (7.9) [or Eq. (7.10)] when one replaces the summation over Γ_0 in Eq. (4.6) with an integration, and when T is large* (as $T \to \infty$ terms with J_0 very large dominate). This result is satisfying and, perhaps, surprising in the very close correspondence it reveals between the quantal and classical results pertaining to rotational coherence.

Having discussed the close similarities between Eqs. (7.9) and (7.10), and Eq. (4.6) at high T, one must hasten to point out that significant differences do exist. First, note that there is a continuum of modulation frequencies in the classical equations, as opposed to discrete frequencies in the quantum case. The presence of a continuum precludes the occurrence of the recurrences that are such a prominent characteristic of decays associated with rotational coherence (see Secs. IV and V). Second, although the quantum beat frequencies approach the classical modulation frequencies in a relative sense, the *absolute* differences in the quantal and classical frequencies are significant. For example, at times $t = n/(2B)$, the quantum beats $\cos[2BJ_0(2\pi)t] = \cos[2B(J_0+1)2\pi t] = 1$, for integer n, while the classical modulation $\cos[2B\sqrt{J_0(J_0+1)}2\pi t]$ approaches $+1$ for n even and -1 for n odd. Therefore, even if one were to *quantize* Eqs. (7.9) and (7.10) by allowing only integer values of J_0 and K_0, the semiclassical equation that would result would not be the same as the quantum decay, even at high T. This point is illustrated in Fig. 8, which shows one decay calculated by using a semiclassical Eq. (7.9) and another decay calculated by using the quantal expression, Eq. (4.6). Clearly, the two decays are very similar in form, both having transients at $n/(2B)$, $n = 0,1,2,\ldots$, and $m/(4B)$, $m = 1,3,5,\ldots$. Nevertheless, there are significant differences between the decays in the neighborhood of the times $t = n/$

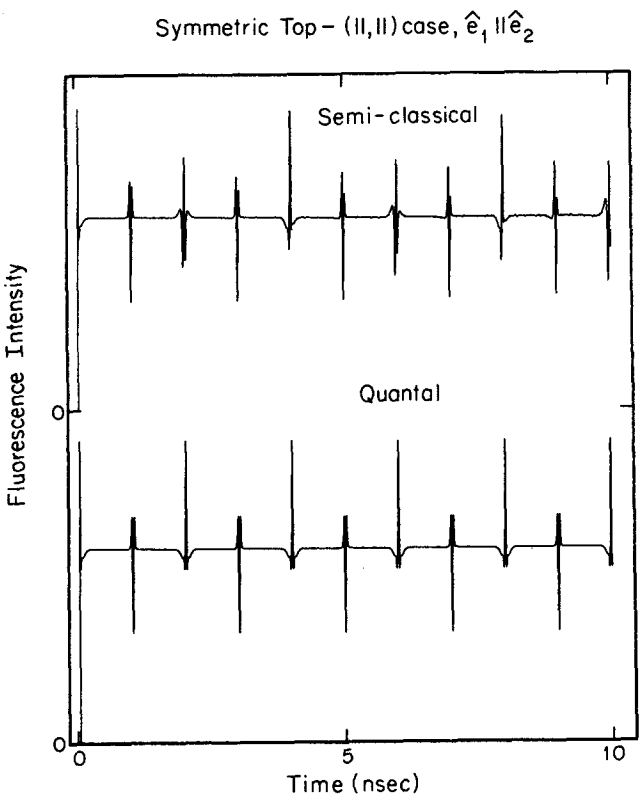

FIG. 8. Calculated fluorescence decays for the (||,||) case of a symmetric top with $\hat{e}_2 \| \hat{e}_1$. For both decays $A = 2.678$ and $B = 0.252$ GHz, $T = 5$ K, $\nu_r = 0.002$ GHz, $\nu_{max} = 99.9$ GHz, $t_r = 1.0$ ps, and $\gamma = 0$. (Top) Decay calculated using a semiclassical version of Eq. (7.9) of the text. (Bottom) Decay calculated using the quantal results of Sec. IV.

$(2B)$, $n = 1,3,5,...$, that is, the times at which $\cos(2BJ_0 2\pi t)$ and $\cos[2B(J_0+1)2\pi t]$ equal $+1$, but at which $\cos[2B\sqrt{J_0(J_0+1)}2\pi t]$ equals -1. The upshot is that the semiclassical treatment of fluorescence from rotating molecules provides an accurate qualitative picture of the manifestations of rotational coherence in time-resolved fluorescence, but the approach is not quantitatively accurate for certain intervals of time in the fluorescence decay.

VIII. ROTATIONAL COHERENCE WITH VIBRATIONAL COHERENCE

Heretofore in this paper we have considered *purely rotational* coherence effects, effects which correspond to situations in which rotational coherence is the only source of quantum interference manifested in an observable. Such situations arise upon the coherent excitation of rotational levels belonging to a single vibronic state manifold (see Secs. IV and V). However, one expects that rotational coherence effects will not always be the only manifestations of quantum coherence in a measured molecular decay. The reason for this expectation is that intramolecular energy relaxation processes, such as intersystem crossing,[20–24] internal conversion,[25] and intramolecular vibrational energy redistribution (IVR),[26] can also give rise to observable coherence effects. In fact, the observation and analysis of such effects has played a large role in the elucidation of the intramolecular couplings from which they arise. Hence, it is pertinent to consider cases in which there are mixed sources of quantum coherence (i.e., rotational coherence/vibrational or electronic coherence), and, as far as one is able, to determine the specifics of how each source contributes to an observed decay. Such information is necessary for the proper interpretation of experimental results and for the efficient design of experimental schemes that will probe what one wishes to probe.

As stated in Sec. III, Eq. (3.19) is an expression that allows for the possibility of mixed coherence effects. To account for vibrational/electronic coherence using Eq. (3.19), one uses a zero-order basis set for the $|\Gamma_1 M_1\rangle$, rather than using molecular eigenstates. Such zero-order states are physically relevant in that they are chosen to be "doorway states" for absorption and emission events. Yet, they do not diagonalize all parts of the molecular Hamiltonian. Therefore, the trace factor in Eq. (3.19) cannot be simplified as in going from Eq. (3.19) to Eq. (3.20); matrix elements containing the nondiagonal portion of the Hamiltonian remain. These matrix elements are what give rise to the energy flow dynamics.

A. Anharmonic coupling

In this subsection we use Eq. (3.19) to consider the simultaneous existence of rotational coherence and the vibrational coherence that arises from anharmonic coupling between vibrational levels in a molecule. The treatment is especially pertinent to our previous work[26] on vibrational coherence and to experimental results to be presented in the companion paper to this one.[8] Moreover, the physical situation is one of the "cleanest" ones to which Eq. (3.19) can be applied, in that the results are quite simple in form. Thus, the analysis may serve as a useful model for the analysis of other cases.

The specifics of the physical situation are shown schematically in Fig. 9. The scheme is a particular case of that

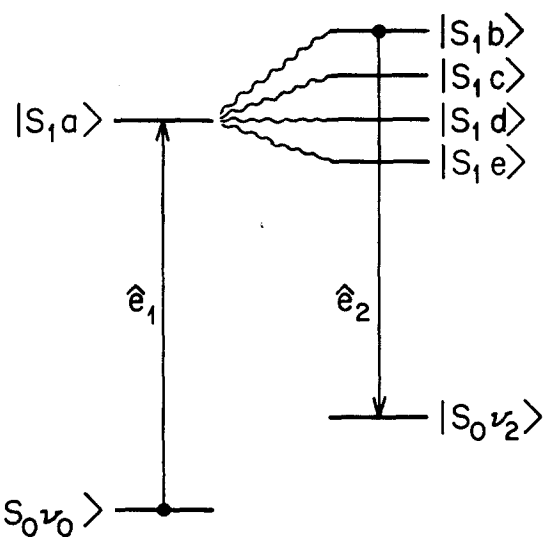

FIG. 9. Level diagram indicating the physical situation treated in Sec. VIII. We assume one relevant initial vibronic state and one relevant final vibronic state. Regarding the excited vibronic states involved, we work in a basis set of coupled zero-order vibronic states in which one vibronic state $|S_1 a\rangle$ has all the absorption strength from $|S_0 \nu_0\rangle$ and one vibronic state $|S_1 b\rangle$ has all the emission strength to $|S_0 \nu_2\rangle$. The rotational manifolds of the vibronic states in the figure are omitted for clarity.

shown in Fig. 2. There is one initial vibronic state $|S_0 v_0\rangle$, one final vibronic state $|S_0 v_2\rangle$, and a number of intermediate vibronic states which are vibrational levels of the S_1 electronic state. The intermediate states are taken to be zero-order ones coupled by anharmonic coupling. Two of these S_1 vibrational levels act as doorway states, the $|S_1 a\rangle$ level as the doorway state in absorption, and the $|S_1 b\rangle$ level as the doorway state in emission. (In other words, only $|S_1 a\rangle$ can be reached in absorption from $|S_0 v_0\rangle$ and only $|S_1 b\rangle$ can emit to $|S_0 v_2\rangle$.)

Anharmonic coupling has the important characteristic that it only depends on the vibrational coordinates of the molecule. Therefore, it does not couple rotational levels with different rotational quantum numbers, and its magnitude does not depend on such quantum numbers. This allows one to choose a rovibronic basis set of states that is diagonal with respect to the rotational part of the molecular Hamiltonian, even though it is not diagonal with respect to the vibrational Hamiltonian. In what follows we shall work in such a basis set. (Note, we have assumed here that the rotational constants of the molecule do not depend on vibrational state. This, from the start, precludes effects arising from rotational constant mismatch.[26(f)])

Let us now consider Eq. (3.19). Under our assumptions, the factor ${}^{\Gamma_1\Gamma_1'}_{L_1 l_1} A^{\Gamma_0\Gamma_0'}_{00}(\hat{e}_1)$ in the equation is only nonzero when the vibronic parts of $|\Gamma_1\rangle$ and $|\Gamma_1'\rangle$ are $|S_1 a\rangle$ (their rotational parts do not have to be the same). Similarly, ${}^{\Gamma_1''\Gamma_1'''}_{L_1' l_1'} A^{\Gamma_2\Gamma_2'}_{00}(\hat{e}_2)$ is nonzero when the vibronic parts of Γ_1'' and Γ_1''' are $|S_1 b\rangle$. Given this, the only pertinent trace factors in Eq. (3.19) are of the form

$$\{\mathrm{Tr}\} = \sum_{M_1 M_1'} \sum_{M_1'' M_1'''} \Bigg[(-1)^{J_1 - M_1} (-1)^{J_1'' - M_1''} (2L_1 + 1)^{1/2} (2L_1' + 1)^{1/2}$$

$$\times \begin{pmatrix} J_1 & L_1 & J_1' \\ M_1 & l_1 & -M_1' \end{pmatrix} \begin{pmatrix} J_1'' & L_1' & J_1''' \\ M_1'' & l_1' & -M_1''' \end{pmatrix} \times \mathrm{Tr}\{e^{-iHt/\hbar} |S_1 a; J_1 \tau_1 M_1\rangle$$

$$\times \langle S_1 a; J_1' \tau_1' M_1' | e^{iHt/\hbar} |S_1 b; J_1''' \tau_1''' M_1'''\rangle \langle S_1 b; J_1'' \tau_1'' M_1'' | \} \Bigg], \tag{8.1}$$

where the expression is valid for symmetric *and* asymmetric tops. (For symmetric tops the τ are just K quantum numbers.) Now, because the $|\Gamma_1\rangle$ basis states diagonalize those parts of the Hamiltonian containing electronic and rotational coordinates, one can simplify Eq. (8.1) into the product of two factors, $g_{er}(t)$ and $g_v(t)$, which depend on electronic and rotational, and vibrational quantum numbers, respectively:

$$g_{er}(t) = e^{-\gamma t} (e^{-i\omega_{\Gamma_1 \Gamma_1' t}}) (\delta_{L_1 L_1'}) (\delta_{l_1 l_1'}) \delta(J_1 J_1' L_1'), \tag{8.2}$$

where we have used Eq. (3.5) and Eq. (3.7.8) of Ref. 30, $\omega_{\Gamma_1\Gamma_1'}$ equals $1/\hbar$ times the *rotational energy difference* between levels $|\Gamma_1\rangle$ and $|\Gamma_1'\rangle$, and the $e^{-\gamma t}$ term represents the decay of all states in the S_1 manifold, and

$$g_v(t) = \mathrm{Tr}_v\{e^{-iH_v t/\hbar} |a\rangle \langle a| e^{iH_v t/\hbar} |b\rangle \langle b|\}, \tag{8.3}$$

where H_v is the vibrational Hamiltonian and Tr_v denotes a trace operation only over S_1 vibrational levels.

One notes now several points. First, $g_v(t)$ can be taken completely outside the Σ sign appearing in Eq. (3.19) since it does not vary with any of the indices of the sum. Second, $g_v(t)$ is just proportional to the decay to be expected[26(d)] given a number of coupled zero-order vibrational levels, one of which ($|a\rangle$) is active in absorption, another ($|b\rangle$) active in emission. To show this, one can evaluate Eq. (8.3) by using S_1 vibrational *eigenstates* $|I\rangle$ to evaluate the trace, and by inserting several projection operators $P_I \equiv \Sigma_I |I\rangle\langle I| = 1$ into the equation to obtain

$$g_v(t) = \sum_{I,I'} e^{-i\omega_{II'} t} \langle I|a\rangle \langle a|I'\rangle \langle I'b\rangle \langle b|I\rangle, \tag{8.4}$$

where $\omega_{II'}$ is $1/\hbar$ times the energy difference between the vibrational eigenstates $|I\rangle$ and $|I'\rangle$. Equation (8.4) is essentially identical to Eq. (2.6) of Ref. 26(d) [apart from the exponential decay term in the latter equation, which term we have included here in $g_{er}(t)$], which describes the manifestations of anharmonically induced vibrational coherence in time-resolved fluorescence. Third, one notes that by taking $g_v(t)$ out of the summation in Eq. (3.19) and by using Eq. (8.2) for $g_{er}(t)$, the summation factor in Eq. (3.19) becomes the same as the right-hand side of Eq. (3.20). Moreover, since only rotational quantum numbers are indices in the summation factor, it is identical to the observables associated with purely rotational coherence. [That is, for symmetric tops, the summation factor is identical to the right-hand side of Eq. (4.5). For asymmetric tops it is the same as the right side of Eq. (5.5).]

The upshot of the above three points is that, in the rotational coherence/anharmonic coupling case considered, *the observable is just the product of a purely vibrational coherence decay and a purely rotational coherence decay*. Moreover, the vibrational coherence factor is identical to what it would be if there were not any rotational level structure to be considered, and the rotational coherence factor is identical to what it would be (1) if there were not vibrational coupling and (2) if only one S_1 vibrational level participated in the absorption and emission processes. The fact that the observable takes the form that it does allows for the easy separation of the manifestations of vibrational dynamics from those of rotational coherence. To obtain the decay reflecting vibrational dynamics, one need only do an experiment with linearly polarized light and with $\hat{e}_1$ at 54.7° with respect to $\hat{e}_2$. (By doing this, the rotational coherence factor becomes constant in time.) On the other hand, the temporal behavior of the fluorescence anisotropy $r(t)$ is determined solely by rota-

tional coherence effects. (The vibrational factor does not depend on polarization.) Thus, by measuring $r(t)$ one observes the manifestations of rotational coherence without any contribution from the vibrational coherence.

B. Coriolis coupling

In closing this section, it is pertinent to briefly consider "rotational coherence" in decays of systems in which Coriolis coupling is present. Assume, as in the preceding subsection, that one vibronic state ($|S_1a\rangle$) has exclusive absorption strength, and that another ($|S_1b\rangle$) has exclusive emission strength. (That is, assume again the situation in Fig. 9 but with the couplings now being Coriolis interactions.) These assumptions again lead to Eq. (8.1) for the trace factor in Eq. (3.19). However, now H is not of the form $H=H_e+H_v+H_r$, as it is in the anharmonic coupling case. Instead $H=H_e+H_{0v}+H_{0r}+H_{vr}$, where the basis functions in Eq. (8.1) are eigenfunctions of the sum of the first three terms in H (but not of H), and where neither H_{0v} nor H_{0r} commutes with H_{vr}. Put another way, H can couple rovibrational states having different vibrational and rotational quantum numbers (ΔJ and ΔM equals zero in the coupling, but $\Delta\tau$ need not), and, moreover, the coupling matrix elements are functions of the rotational quantum numbers.

Equation (8.1), together with the Coriolis selection rules on J and M, becomes

$$\begin{aligned}\mathrm{Tr}=&e^{-rt}(\delta_{L_1,L_1'})(\delta_{I_1,I_1'})\delta(J_1J_1'L_1')\\&\times\mathrm{Tr}\{e^{-iH_{vr}'t/\hbar}|a;J_1\tau_1\rangle\\&\times\langle a;J_1'\tau_1'|e^{iH_{vr}'t/\hbar}|b;J_1'\tau_1'''\rangle\langle b;J_1\tau_1''|\},\end{aligned}\tag{8.5}$$

where $H_{vr}'\equiv H_{0v}+H_{0r}+H_{vr}$. One notes the principal point: One cannot, in general, separate Eq. (8.5) into two factors that depend exclusively on rotational and vibrational quantum numbers, respectively [i.e., into analogs of Eqs. (8.2) and (8.3)]. Unlike the anharmonic case, for which one can speak of separable contributions from purely vibrational and purely rotational coherence, for the Coriolis case one must speak of rovibrational coherence. Thus, it is evident that the situation gives rise to observable manifestations in time-resolved fluorescence polarization experiments that are considerably more complicated in form than the manifestations of (1) purely rotational coherence or (2) anharmonic coupling interactions. The formalism presented in this paper can readily be applied to the Coriolis coupling case, once the exact nature of the coupling Hamiltonian is determined.

IX. CONCLUSIONS

In this paper we have developed a theory describing the manifestations of what we term *purely rotational coherence.* It is shown for a wide variety of possible cases encompassing different absorption and emission dipole directions, different excitation and detection polarizations, different molecular geometries, and different temperatures, that such manifestations should be observable as transients and recurrences (spaced by time intervals that depend on the rotational constants of the molecule) in picosecond-resolved, polarization-analyzed fluorescence. Thermal averaging does not preclude their observation. This being the case, the phenomenon of rotational coherence represents a new and potentially very fruitful technique by which to probe the spectroscopy and dynamics of vibronically excited molecules. One area in particular, that of the sub-Doppler, high resolution determination of rotational constants, has been explored by us in previous letters[1,2] and is fully developed in the accompanying paper.[8]

Herein, we have also made an attempt to develop a physical picture of purely rotational coherence in isolated molecules as a phenomenon reflecting the time-dependent orientation of excited molecules in a gaseous sample. In this same vein, we have compared the characteristics of the observables associated with the phenomenon to those to be expected from classically rotating molecules and from molecules undergoing rotational diffusion in liquids. Close similarities exist between all these situations, similarities that, for instance, give rise to identical $r(0)$ values in the different situations and to the fact that magic angle detection eliminates all vestiges of rotational dynamics in the time-resolved fluorescence corresponding to the different situations.

Third, our results show that rotational coherence effects can contribute in significant ways to decays that also contain coherence effects associated with intramolecular relaxation phenomena. For the particular case in which the relaxation is intramolecular vibrational energy redistribution arising from anharmonic coupling between zero-order vibrational levels in an excited electronic state manifold, it is also shown that the mixed coherence effects can be readily separated simply by varying the polarization scheme of the experiment.

Finally, we have developed a general capability of calculating the decays to be expected in different situations involving purely rotational coherence. This capability can be very useful as a guide in designing, performing, and interpreting experiments, as we shall demonstrate in the accompanying paper.[8]

ACKNOWEDGMENTS

It is our pleasure to acknowledge F. A. Perez and J. S. Baskin for their contributions to this work.

APPENDIX

The aim in this Appendix is to present the derivation of Eq. (4.12) $-r(t)$ for the case of a symmetric top with μ_1 and μ_2 parallel to the symmetry axis of the molecule. We shall use Eq. (4.6) along with the results of Table I. If one assumes that $G(\Gamma_0)=1$ for all Γ_0 one has

$$r(t)=\frac{S_1+S_2(t)}{S_3},\tag{A1}$$

where

$$S_1\equiv\sum_{\Gamma_0}\sum_{J_1}e^{-E_{\Gamma_0}/k_BT}\left[f_{\parallel}(J_0,J_1,J_1,K_0)-f_{\perp}(J_0,J_1,J_1,K_0)\right],\tag{A2}$$

$$S_2 \equiv 2 \sum_{\Gamma_0} \sum_{J_1 > J_1'} e^{-E_{\Gamma_0}/k_B T} [\, f_{\parallel}(J_0,J_1,J_1',K_0) - f_{\perp}(J_0,J_1,J_1',K_0)\,] \cos(\omega_{\Gamma_1\Gamma_1'} t), \tag{A3}$$

and

$$S_3 \equiv \sum_{\Gamma_0} \sum_{J_1} e^{-E_{\Gamma_0}/k_B T} [\, f_{\parallel}(J_0,J_1,J_1,K_0) + 2 f_{\perp}(J_0,J_1,J_1,K_0)\,]. \tag{A4}$$

In Eq. (A1) we have made use of Eq. (4.8) and of the fact that $f_{\parallel} + 2f_{\perp}$ is nonzero only for $J_1 = J_1'$.

To determine $r(t)$ we shall approximate the summations over Γ_0 in Eqs. (A2)–(A4) as integrals over J_0 and K_0. We also shall assume that terms with $J_0 \gg 1$ are the only important ones. Hence, we set factors like $(J_0 + 1)$ and $(J_0 + 2)$ equal to J_0 in the expressions for the f values, the $\omega_{\Gamma_1\Gamma_1'}$, and the Boltzmann factor. With these approximations, using Table I,

$$S_1 = \frac{1}{15} \int_0^{\infty} 2 \int_0^{J_0} \left(9 \frac{K_0^4}{J_0^3} - 6 \frac{K_0^2}{J_0} + J_0 \right) \times e^{-\beta K_0^2} e^{-\alpha J_0^2} dK_0\, dJ_0, \tag{A5}$$

$$S_2 = \frac{2}{5} \int_0^{\infty} 2 \int_0^{J_0} \left[\frac{2K_0^2 (J_0^2 - K_0^2)}{J_0^3} \cos(4\delta J_0) + \frac{(J_0^2 - K_0^2)^2}{2J_0^3} \cos(8\delta J_0) \right] \times e^{-\beta K_0^2} e^{-\alpha J_0^2} dK_0\, dJ_0, \tag{A6}$$

and

$$S_3 = \frac{1}{3} \int_0^{\infty} 2 \int_0^{J_0} 2J_0\, e^{-\beta K_0^2} e^{-\alpha J_0^2} dK_0\, dJ_0, \tag{A7}$$

where we have used the fact that the integrands are even in K_0 and have defined $\alpha \equiv B/k_B T$, $\beta \equiv (A - B)/k_B T$, and $\delta \equiv \pi B t$.

Now the integrals over K_0 can be evaluated in terms of the incomplete gamma function[39] $\gamma(1/2,x)$:

$$\int_0^{J_0} (K_0)^n e^{-\beta K_0^2} dK_0 = \frac{\gamma[(n+1)/2, \beta J_0^2]}{2\beta^{(n+1)/2}}. \tag{A8}$$

The remaining integrals over J_0 are of the form

$$\frac{1}{2\beta^{(n+1)/2}} \int_0^{\infty} J_0^m \gamma[(n+1)/2, \beta J_0^2] \times \cos(k\delta J_0) e^{-\alpha J_0^2} dJ_0, \tag{A9}$$

where $k = 0$, 4, or 8. Integrals such as Eq. (A9) can be evaluated using the Gaussian–Laguerre numerical method.[41] They approximate

$$\frac{1}{4\beta^{(n+1)/2} \alpha^{(m+1)/2}} \sum_{i=1}^{N} w_i (y_i)^{(m-1)/2} \times \gamma[(n+1)/2, \beta y_i/\alpha] \cos(k\delta \sqrt{y_i/\alpha}), \tag{A10}$$

where the w_i's and y_i's are constants which depend on N,[42] and where the approximation is better the larger N.

The next task is to evaluate the incomplete gamma functions. From Eqs. (A5)–(A7) it is apparent that we need be concerned only with those γ functions for which $(n + 1/2) = 1/2$, 3/2, and 5/2. For the latter two values the function can be expressed in terms of $\gamma(\frac{1}{2},x)$ [43]:

$$\gamma(3/2,x) = \frac{\gamma(\frac{1}{2},x)}{2} - (x)^{1/2} e^{-x}, \tag{A11}$$

$$\gamma(5/2,x) = \frac{3\gamma(\frac{1}{2},x)}{4} - \left[\frac{3}{2} (x)^{1/2} + (x)^{3/2} \right] e^{-x}. \tag{A12}$$

Eventually, $\gamma(\frac{1}{2},x)$ can be evaluated numerically.[44] With Eq. (A8), and Eqs. (A10)–(A12), Eqs. (A5)–(A7) become

$$S_1 = \frac{1}{120\alpha\beta^{1/2}} \sum_{i=1}^{N} w_i \{[27(x_i)^{-2} - 12(x_i)^{-1} + 4]\gamma(1/2,x_i) - [54(x_i)^{-3/2} + 12(x_i)^{-1/2}] e^{-x_i}\}, \tag{A13}$$

$$S_2 = \frac{1}{10\alpha\beta^{1/2}} \sum_{i=1}^{N} w_i \cos(4\pi t \sqrt{Bk_B T y_i}) \{[2(x_i)^{-1} - 3(x_i)^{-2}]\gamma(1/2,x_i) + 6(x_i)^{-3/2} e^{-x_i}\} + \frac{1}{40\alpha\beta^{1/2}} \sum_{i=1}^{N} w_i \cos(8\pi t \sqrt{Bk_B T y_i}) \times \{[4 - 4(x_i)^{-1} + 3(x_i)^{-2}]\gamma(1/2,x_i) + [4(x_i)^{-1/2} - 6(x_i)^{-3/2}] e^{-x_i}\}, \tag{A14}$$

$$S_3 = \frac{1}{3\alpha\beta^{1/2}} \sum_{i=1}^{N} w_i \gamma(1/2,x_i), \tag{A15}$$

where we have defined $x_i \equiv (\beta y_i/\alpha) = (A - B) y_i/B$. Eqs. (A13)–(A15), together with Eq. (A1), give Eq. (4.12) with terms in the latter defined as follows:

$$K \equiv \frac{S_1}{S_3}, \tag{A16}$$

$$g_i(A,B) = \frac{3}{10} \frac{w_i \{[2(x_i)^{-1} - 3(x_i)^{-2}]\gamma(\frac{1}{2},x_i) + 6(x_i)^{-3/2} e^{-x_i}\}}{\sum_{j=1}^{N} w_j \gamma(\frac{1}{2},x_j)}, \tag{A17}$$

and

$$h_i(A,B) = \frac{3}{40} \frac{w_i \{[4 - 4(x_i)^{-1} + 3(x_i)^{-2}]\gamma(\frac{1}{2},x_i) + [4(x_i)^{-1/2} - 6(x_i)^{-3/2}] e^{-x_i}\}}{\sum_{j=1}^{N} w_j \gamma(\frac{1}{2},x_j)}. \tag{A18}$$

[1]P. M. Felker, J. S. Baskin, and A. H. Zewail, J. Phys. Chem. **90**, 724 (1986).
[2]J. S. Baskin, P. M. Felker, and A. H. Zewail, J. Chem. Phys. **84**, 4708 (1986).
[3]For reviews, see: (a) S. Haroche, in *High Resolution Laser Spectroscopy*, edited by K. Shimoda (Springer, Berlin, 1976); (b) J. N. Dodd and G. W. Series, in *Progress in Atomic Spectroscopy, Part A*, edited by W. Hanle and H. Kleinpoppen (Plenum, New York, 1978); (c) R. N. Zare, Acc. Chem. Res. **4**, 361 (1971).
[4](a) Y. Matsumoto, L. H. Spangler, and D. W. Pratt, Chem. Phys. Lett. **95**, 343 (1983); (b) **98**, 333 (1983).
[5](a) J. W. Perry, N. F. Scherer, and A. H. Zewail, Chem. Phys. Lett. **103**, 1 (1983); (b) N. F. Scherer, J. F. Shepanski, and A. H. Zewail, J. Chem. Phys. **81**, 2181 (1984).
[6](a) D. K. Negus, D. S. Green, and R. M. Hochstrasser, Chem. Phys. Lett. **117**, 409 (1985); (b) A. J. Bain, P. J. McCarthy, and R. M. Hochstrasser, *ibid.* **125**, 307 (1986). Note that in Ref. 6(b) a value of 48 ± 8 ps is quoted as the "rotational relaxation time" of *t*-stilbene in a high temperature bulb. In a private communication (to be published), the authors of the paper have indicated that the value corresponds instead to population decay of the excited molecules. We mention this because the decay simulations we present herein and the experimental results of Ref. 8 give much shorter anisotropy decay times, consistent with the earlier work (Ref. 5).
[7](a) G. M. Nathanson and G. M. McClelland, J. Chem. Phys. **81**, 629 (1985); (b) **84**, 3170 (1986).
[8]J. S. Baskin, P. M. Felker, and A. H. Zewail, J. Chem. Phys. **86**, 2483 (1987).
[9](a) M. P. Silverman, S. Haroche, and M. Gross, Phys. Rev. A **18**, 1507 (1978); (b) **18**, 1517 (1978).
[10]G. Herzberg, *Molecular Spectra and Molecular Structure* (Van Nostrand–Reinhold, New York, 1966), Vol. III.
[11](a) S. Haroche, J. A. Paisner, and A. L. Schawlow, Phys. Rev. Lett. **30**, 948 (1973); (b) R. Wallenstein, J. A. Paisner, and A. L. Schawlow, *ibid.* **32**, 1333 (1974).
[12]W. Gornik, D. Kaiser, J. Luther, and H. H. Schultz, Opt. Commun. **6**, 948 (1972).
[13]A. Corney and G. W. Series, Proc. Phys. Soc. London **83**, 207 (1964).
[14]H. J. Andra, Phys. Rev. Lett. **25**, 325 (1970).
[15]P. Schenck, R. C. Hilborn, and H. Metcalf, Phys. Rev. Lett. **31**, 189 (1973).
[16]T. W. Ducas, M. G. Littman, and M. L. Zimmerman, Phys. Rev. Lett. **35**, 1752 (1975).
[17](a) P. J. Brucat and R. N. Zare, J. Chem. Phys. **78**, 100 (1983); (b) **81**, 2562 (1984); (c) Mol. Phys. **55**, 277 (1985).
[18](a) J. Muhlbach, M. Dubs, H. Bitto, and J. R. Huber, Chem. Phys. Lett. **111**, 288 (1984); (b) M. Dubs, J. Muhlbach, H. Bitto, P. Schmidt, and J. R. Huber, J. Chem. Phys. **83**, 3755 (1985).
[19](a) J. P. Heritage, T. K. Gustafson, and C. H. Lin, Phys. Rev. Lett. **34**, 1299 (1975); (b) T. K. Yee and T. K. Gustafson, Phys. Rev. A **18**, 1597 (1978).
[20](a) J. Chaiken, T. Benson, M. Gurnick, and J. D. McDonald, Chem. Phys. Lett. **61**, 195 (1979); (b) J. Chaiken, M. Gurnick, and J. D. McDonald, J. Chem. Phys. **74**, 106 (1981); (c) J. Chaiken and J. D. McDonald, *ibid.* **77**, 669 (1982).
[21]H. Henke, H. L. Selzle, T. R. Hays, S. H. Lin, and E. W. Schlag, Chem. Phys. Lett. **77**, 448 (1981).
[22]S. Okajima, H. Saigusa, and E. C. Lim, J. Chem. Phys. **76**, 2096 (1982).
[23]B. J. van der Meer, H. T. Jonkman, G. M. ter Horst, and J. Kommandeur, J. Chem. Phys. **76**, 2099 (1982).
[24]P. M. Felker, W. R. Lambert, and A. H. Zewail, Chem. Phys. Lett. **89**, 309 (1982).
[25](a) W. Sharfin, M. Ivanco, and S. C. Wallace, J. Chem. Phys. **76**, 2095 (1982); (b) M. Ivanco, J. Hager, W. Sharfin, and S. C. Wallace, *ibid.* **78**, 6531 (1983).
[26](a) W. R. Lambert, P. M. Felker, and A. H. Zewail, J. Chem. Phys. **75**, 5958 (1981); (b) P. M. Felker and A. H. Zewail, Chem. Phys. Lett. **102**, 113 (1983); (c) Phys. Rev. Lett. **53**, 501 (1984); (d) J. Chem. Phys. **82**, 2961 (1985); (e) **82**, 2975 (1985); (f) **82**, 2994 (1985); (g) **82**, 3003 (1985).
[27]We emphasize that the theory herein pertains to spatially isotropic samples. Spatial isotropy need not always characterize molecular beam samples. For example, see M. P. Sinha, C. D. Caldwell, and R. N. Zare, J. Chem. Phys. **61**, 491 (1974); and A. G. Visser, J. P. Kekooy, L. K. van der Meij, C. de Vreugd, and J. Korving, Chem. Phys. **20**, 391 (1977).
[28]For a thorough treatment of saturation effects on atomic quantum beats see Ref. 9(a).
[29]The Euler angles are defined with the convention used in Ref. 30.
[30]A. R. Edmonds, *Angular Momentum in Quantum Mechanics* (Princeton University, Princeton, 1968).
[31]Note that we are assuming that all states $|\Gamma_i M_i\rangle$ in the *i*th manifold decay at the same rate. Of course, this need not be true. Both diagonal and off-diagonal elements of the tensor operators may have different relaxation rates. However, for rotational levels of a given vibronic state of an *isolated* molecule, the approximation is reasonable. One notes that if the approximation is not valid, the generalization of the theory is straightforward.
[32]Equation (3.21) was derived from Eq. (17) of Ref. 9(b) for the particular types of A factors appearing in Eqs. (3.19) and (3.20) of this paper.
[33]For example, see (a) T. J. Chuang and K. B. Eisenthal, J. Chem. Phys. **57**, 5094 (1972); (b) A. J. Cross and G. R. Fleming, Biophys. J. **46**, 45 (1984).
[34]G. W. Loge and C. S. Parmenter, J. Chem. Phys. **74**, 29 (1981).
[35]C. H. Townes and A. L. Schawlow, *Microwave Spectroscopy* (Dover, New York, 1975).
[36]For example, R. G. Gordon, J. Chem. Phys. **43**, 1307 (1965).
[37]D. A. McQuarrie, *Statistical Mechanics* (Harper and Row, New York, 1976), p. 485.
[38]For example, see (a) H. Goldstein, *Classical Mechanics* (Addison-Wesley, Reading, MA, 1950); (b) L. D. Landau and E. M. Lifshitz, *Mechanics*, 3rd ed. (Permagon, Oxford, 1976).
[39]Equation (6.5.2), p. 260 of Ref. 40.
[40]*Handbook of Mathematical Functions*, edited by M. Abramowitz and I. E. Stegun, National Bureau of Standards (U. S. GPO, Washington, D. C., 1972).
[41]Equation (25.4.45), p. 890 of Ref. 40.
[42]Table 25.9, p. 923 of Ref. 40.
[43]Equation (6.5.22), p. 262 of Ref. 40.
[44]Equation (6.5.16), p. 262, or Eq. (26.4.19), p. 941 of Ref. 40.